Circ J 2009; **73:** 851–859

Servo-Controlled Hind-Limb Electrical Stimulation for Short-Term Arterial Pressure Control

Toru Kawada, MD; Shuji Shimizu, MD; Hiromi Yamamoto, MD*;
Toshiaki Shishido, MD; Atsunori Kamiya, MD; Tadayoshi Miyamoto, PhD**;
Kenji Sunagawa, MD†; Masaru Sugimachi, MD

Background: Autonomic neural intervention is a promising tool for modulating the circulatory system thereby treating some cardiovascular diseases.

Methods and Results: In 8 pentobarbital-anesthetized cats, it was examined whether the arterial pressure (AP) could be controlled by acupuncture-like hind-limb electrical stimulation (HES). With a 0.5-ms pulse width, HES monotonically reduced AP as the stimulus current increased from 1 to 5 mA, suggesting that the stimulus current could be a primary control variable. In contrast, the depressor effect of HES showed a nadir approximately 10 Hz in the frequency range between 1 and 100 Hz. Dynamic characteristics of the AP response to HES approximated a second-order low-pass filter with dead time (gain: −10.2±1.6 mmHg/mA, natural frequency: 0.040±0.004 Hz, damping ratio 1.80±0.24, dead time: 1.38±0.13 s, mean±SE). Based on these dynamic characteristics, a servo-controlled HES system was developed. When a target AP value was set at 20 mmHg below the baseline AP, the time required for the AP response to reach 90% of the target level was 38±10 s. The steady-state error between the measured and target AP values was 1.3±0.1 mmHg.

Conclusions: Autonomic neural intervention by acupuncture-like HES might provide an additional modality to quantitatively control the circulatory system. (*Circ J* 2009; **73:** 851–859)

Key Words: Proportional-integral controller; Transfer function

Because abnormality in the autonomic nervous system is often associated with cardiovascular diseases, treating cardiovascular diseases by autonomic neural interventions have attracted many researchers![1–6] Recently, autonomic neural interventions using electronic devices have again gained the focus of attention as a potential modality for treating cardiovascular diseases resistant to conventional therapeutics. To name a few, chronic vagal nerve stimulation dramatically improves the survival of chronic heart failure after myocardial infarction in rats[7] Chronic baroreceptor activation enhances the survival of pacing-induced heart failure in dogs[8] A recent version of a device-based treatment of hypertension in human is reported[9] A framework of electrical neural intervention is also effective to elevate arterial pressure (AP) against hypotensive events![10–13]

Aside from direct neural stimulation, electroacupuncture can modify autonomic balance, thereby treating cardiovascular diseases![14–16] Although one feature of the electroacupuncture might be its long-lasting effects, immediate cardiovascular responses to acupuncture-like stimulation are also observed in several experimental settings. For example, a 60-s manual acupuncture-like stimulation of a hind limb reduces renal or cardiac sympathetic nerve activity, causing hypotension and bradycardia in anesthetized rats![17,18] We have shown that electrical stimulation of a hind limb using acupuncture needles immediately resets the arterial baroreflex and reduces sympathetic nerve activity in anesthetized rabbits![19] Acupuncture-like hind-limb electrical stimulation (HES) induces immediate hypotension with changes in the relationship between cardiac and renal sympathetic nerve activities in anesthetized cats![20]

In the present study, we hypothesized that AP could be controlled by HES. Quantification of the dynamic input–output relationship between a given stimulus and the AP response is essential for artificially controlling AP![10–12] Accordingly, the first aim was to identify the dynamic input–output relationship between HES and the AP response. The second aim was to develop a feedback controller system that could reduce AP at a prescribed target level using HES.

Methods

Surgical Preparation

Animal care was provided in strict accordance with the *Guiding Principles for the Care and Use of Animals in the Field of Physiological Sciences,* approved by the Physiological Society of Japan. All protocols were approved by the Animal Subject Committee of the National Cardiovascular Center. Eight adult cats weighing from 2.3 to 4.3 kg were

(Received November 17, 2008; revised manuscript received December 10, 2008; accepted December 21, 2008; released online March 18, 2009)

*Department of Cardiovascular Dynamics, Advanced Medical Engineering Center, National Cardiovascular Center Research Institute, Suita, *Division of Cardiology, Department of Internal Medicine, Kinki University School of Medicine, Osakasayama, **Department of Physical Therapy, Faculty of Health Sciences, Morinomiya University of Medical Sciences, Osaka and †Department of Cardiovascular Medicine, Graduate School of Medical Sciences, Kyushu University, Fukuoka, Japan*

Mailing address: Toru Kawada, MD, Department of Cardiovascular Dynamics, Advanced Medical Engineering Center, National Cardiovascular Center Research Institute, 5-7-1 Fujishirodai, Suita 565-8565, Japan. E-mail torukawa@res.ncvc.go.jp

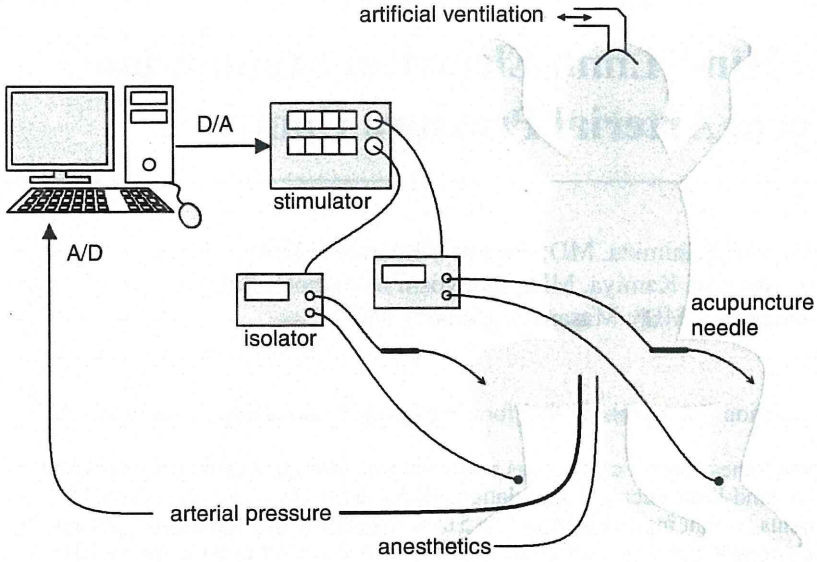

Figure 1. Experimental setup.

anesthetized by an intraperitoneal injection of pentobarbital sodium (30–35 mg/kg) and ventilated mechanically via a tracheal tube with oxygen-supplied room air. The depth of anesthesia was maintained with a continuous intravenous infusion of pentobarbital sodium (1–2 mg·kg^{-1}·h^{-1}) through a catheter inserted into the right femoral vein. Vecuronium bromide (0.5–1.0 mg·kg^{-1}·h^{-1}, iv) was given continuously to suppress muscular activity. AP was measured using a catheter-tip manometer inserted from the right femoral artery and advanced into the thoracic aorta.

HES

In the supine position, both hind limbs were lifted to obtain a better view of the lateral sides of the lower legs. An acupuncture needle with a diameter of 0.2 mm (CE0123, Seirin-Kasei, Shimizu, Japan) was inserted into a point below the knee joint just lateral to the tibia[20] A 23-gauge needle was inserted into the skin behind the ankle as the ground. HES was applied bilaterally via 2 independent isolators connected to an electrical stimulator (SEN 7203, Nihon Kohden, Tokyo, Japan) as shown in **Figure 1**. The pulse width was changed manually whereas the stimulus frequency and the stimulus current were controlled by a dedicated laboratory computer system. The electrical stimulation was started after the hemodynamic effects of needle insertion had disappeared, and the acupuncture needle remained inserted during each protocol.

Protocols

Protocol 1 (n=8) To quantify the AP response to HES as a function of stimulus current and pulse width, we fixed the stimulus frequency at 10 Hz and changed the stimulus current stepwise from 0 to 5 mA in 1-mA increments every minute. The 6-min current test was repeated with an intervening interval of 3–5 min using different pulse widths (0.1, 0.2, 0.5 and 1 ms). The order of the pulse-width settings was randomized across the animals.

Protocol 2 (n=8) To quantify the AP response to HES as a function of stimulus frequency and pulse width, we fixed the stimulus current at 3 mA and changed the stimulus frequency sequentially from 0 to 100 Hz (0, 1, 2, 5, 10, 15, 20, 50 and 100 Hz). Each stimulus frequency was maintained for 1 min. The 9-min frequency test was repeated with an intervening interval of 3–5 min using different pulse widths (0.1, 0.2, 0.5 and 1 ms). The order of the pulse-width settings was randomized across the animals.

Protocol 3 (n=8) To identify the dynamic input–output relationship between HES and the AP response, we randomly turned HES on and off every 2 s according to a binary white noise sequence for 30 min. The HES setting (0.5-ms pulse width, 10 Hz, 3 mA) was chosen to induce effective hypotension based on the preliminary results obtained from Protocols 1 and 2.

Protocol 4 (n=8) Based on the result of Protocol 3, we designed a feedback controller that could automatically adjust the stimulus frequency and the stimulus current for HES. The pulse width was fixed at 0.5 ms. To examine the performance of the feedback controller, we set a target AP value at 20 mmHg below the baseline AP and activated the feedback controller for 10 min.

The following 2 supplemental protocols were performed in 3 of the 8 cats: (1) we inserted 2 acupuncture needles into the triceps surae muscle with a distance of approximately 2.5 cm, and examined if changes in AP was associated with direct muscle stimulation (0.5-ms pulse width, 10 Hz, 3 mA). Both hind limbs were stimulated simultaneously using 2 independent isolators; and (2) we exposed the sciatic nerve after finishing Protocols 1 through 4, and examined if sectioning the sciatic nerve abolished the hemodynamic effects of HES. Unilateral HES was performed (0.5-ms pulse width, 10 Hz, 3 mA) before and after sectioning the ipsilateral sciatic nerve.

Data Analysis

In Protocols 1 and 2, the AP value was obtained by averaging the last 10-s data at each stimulus condition. In Protocol 1, the effect of stimulus current was assessed by changes in AP from the 0-mA stimulus condition for each pulse width. In Protocol 2, the effect of stimulus frequency was assessed by changes in AP from the 0-Hz stimulus condition for each pulse width.

In Protocol 3, the transfer function from HES to AP was estimated by means of an analysis for one-input, one-output systems. Data were first resampled at 10 Hz and segmented into 8 sets of 50%-overlapping bins of 4,096 points each. For each segment, a linear trend was subtracted and a

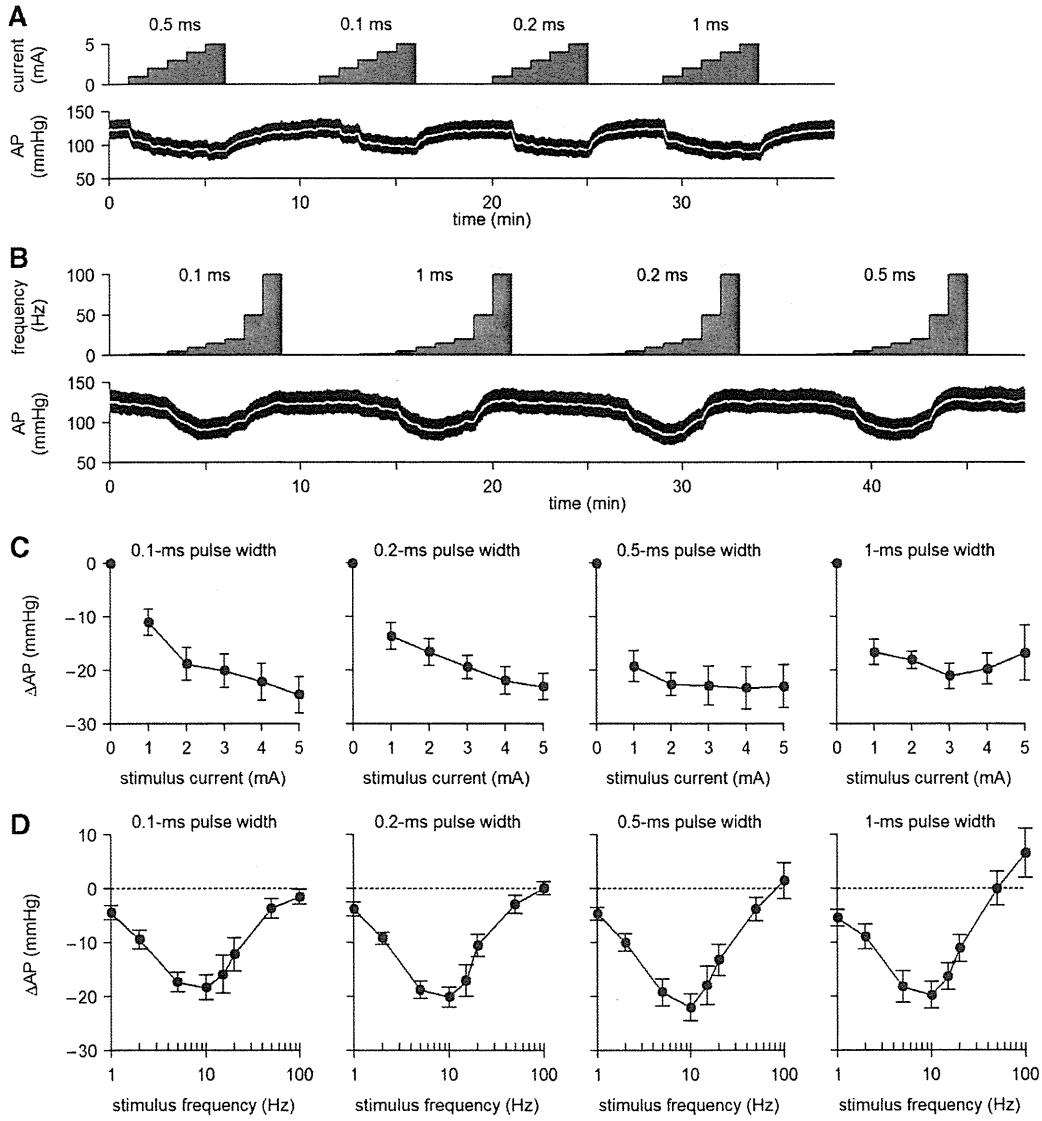

Figure 2. (**A**) Typical recordings of Protocol 1 showing the effects of stimulus current and pulse width on arterial pressure (AP). (**B**) Typical recordings of Protocol 2 showing the effects of stimulus frequency and pulse width on AP. The white lines in the AP traces indicate 2-s moving averaged data. (**C**) Changes in AP as a function of the stimulus current. AP decreased monotonously as the stimulus current increased ($P<0.05$). (**D**) Changes in AP as a function of the stimulus frequency. AP decreased more as the stimulus frequency increased from 1 to 10 Hz but the depressor effect became smaller when the stimulus frequency exceeded 10 Hz ($P<0.05$).

Hanning window was applied. Frequency spectra of the input and output were obtained via fast Fourier transformation. Next, the ensemble averages of input power spectral density [$Sxx(f)$], output power spectral density [$Syy(f)$], and cross spectral density between the input and output [$Syx(f)$] were calculated over the 8 segments. Finally, the transfer function from input to output [$H(f)$] was calculated as:[21]

$$H(f)=\frac{Syx(f)}{Sxx(f)} \quad (1)$$

To quantify the linear dependence between the input and output signals in the frequency domain, a magnitude-squared coherence function [$Coh(f)$] was also calculated as:[21]

$$Coh(f)=\frac{|Syx(f)|^2}{Sxx(f)Syy(f)} \quad (2)$$

In Protocol 4, the performance of the feedback controller was evaluated by the time required for the AP response to reach 90% of the target AP decrease and by the standard deviation of the steady-state error between the target and measured AP values during the last 5 min of the 10-min feedback control. These 2 values were calculated based on the 2-s moving averaged data of AP.

Statistical Analysis

All data are presented as mean and SE values. In Protocol 1, changes in AP were examined by 2-way repeated-measures analysis of variance (ANOVA) using the stimulus current as one factor and the pulse width as the other factor.[22] In Protocol 2, changes in AP were examined by 2-way repeated-measures ANOVA using the stimulus frequency as one factor and the pulse width as the other factor. Differences were considered significant when $P<0.05$.

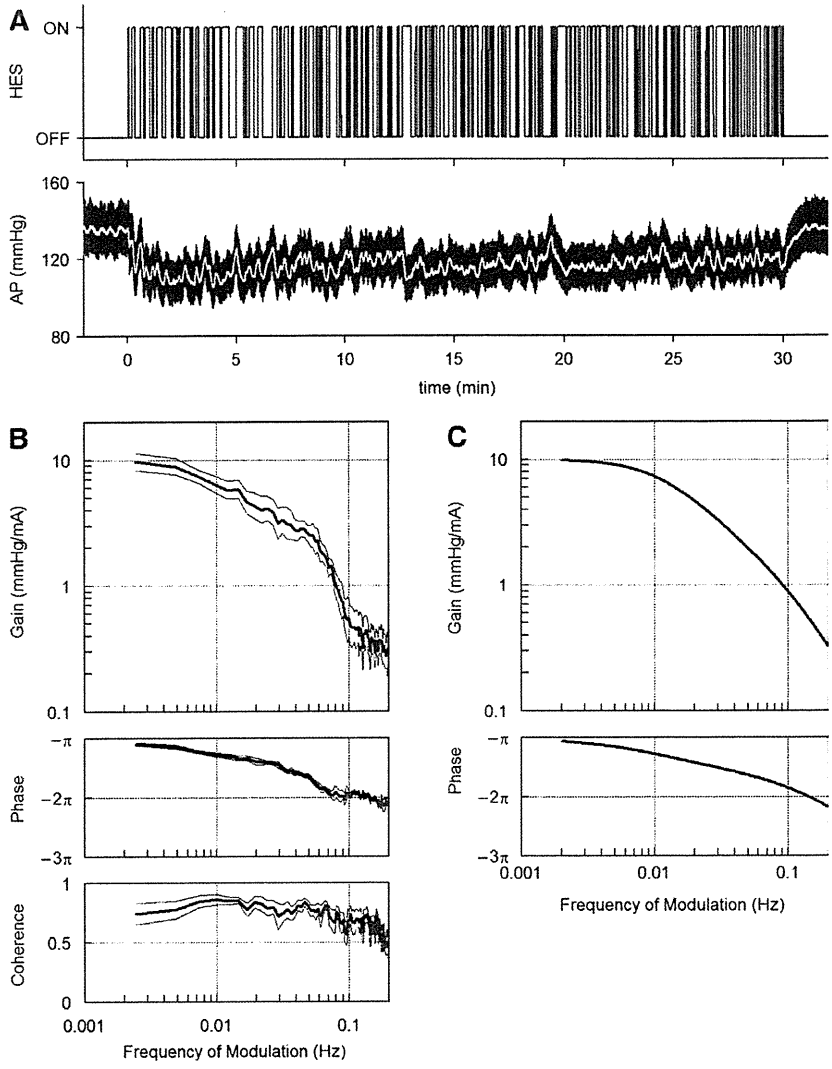

Figure 3. (**A**) Typical recordings of random hind-limb electrical stimulation (HES) and arterial pressure (AP) response. (**B**) Transfer function from HES to the AP response averaged from 8 cats. Thick and thin lines indicate mean and mean±SE values, respectively. (**C**) A model transfer function of the second-order low-pass filter with a lag time that mimics the transfer function from HES to AP.

Results

Relationship Between Stimulus Intensity and AP Response

Typical time series of Protocols 1 and 2 obtained from one animal are shown in **Figures 2A** and **B**, respectively. The pulse width was set in a random order. In Protocol 1, baseline AP obtained at the 0-mA stimulus condition was 118.4±5.4 mmHg across the animals. Changes in mean AP as a function of stimulus current are summarized in **Figure 2C**. The decrease in AP became greater as the stimulus current increased. The overall statistical analysis indicated that the effect of the stimulus current on the magnitude of AP decrease was significant whereas that of pulse width was not. There was no significant interaction effect between the stimulus current and the pulse width.

In Protocol 2, baseline AP at the 0-Hz stimulus condition was 117.6±5.9 mmHg across the animals. Changes in mean AP as a function of stimulus frequency are summarized in **Figure 2D**. The decrease in AP became greater as the stimulus frequency increased from 1 to 10 Hz but it became smaller when the stimulus frequency exceeded 10 Hz. At the pulse width of 1 ms, the stimulus frequency of 100 Hz even increased AP. The overall statistical analysis indicated that the effect of stimulus frequency on the magnitude of AP decrease was significant whereas that of pulse width was not. There was no significant interaction effect between the stimulus frequency and the pulse width.

Dynamic Characteristics of AP Response to HES

Figure 3A depicts a typical time series obtained from Protocol 3. HES was turned on and off randomly, which decreased the mean level of AP and also caused intermittent AP variations. When HES was finally turned off at 30 min, AP began to increase toward the prestimulation value. A long-lasting effect of HES was not observed in the present protocol. The white line in the AP trace represents the 2-s moving averaged data of AP.

The results of transfer function analysis are depicted in **Figure 3B**. In the gain plot, the magnitude of AP response relative to the HES input was plotted in the frequency domain. The gain value became smaller as the frequency increased, indicating the low-pass characteristics of the AP response to HES. In the phase plot, AP showed an out-of-phase relationship with HES at the lowest frequency (0.0024 Hz). The phase delayed more with increasing the frequency of modulation. The coherence value was approximately 0.7 in the frequency range below 0.06 Hz. The

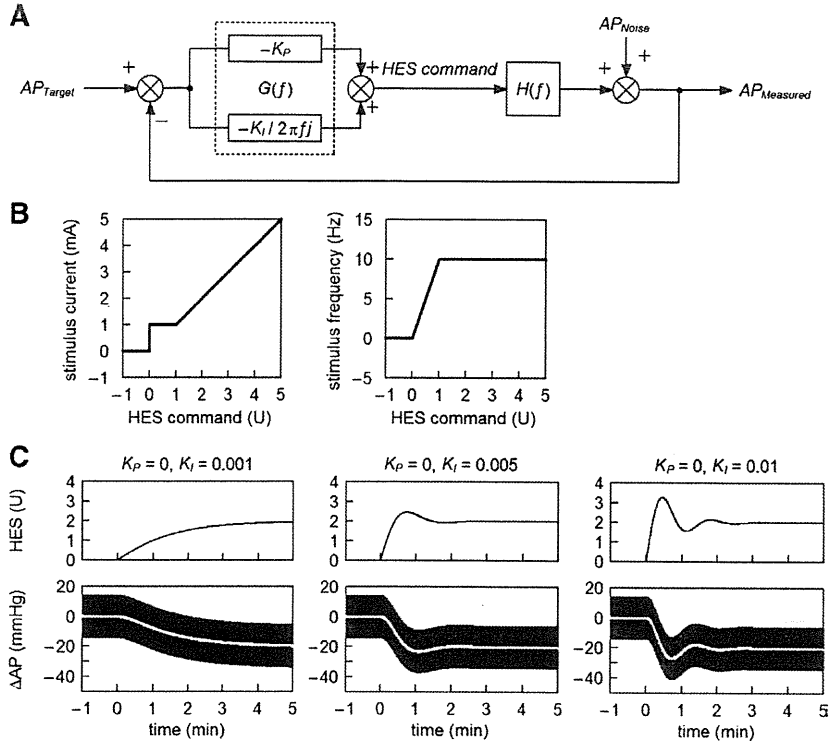

Figure 4. (**A**) A simplified diagram of the feedback controller utilized in the present study. AP_{Target}: target arterial pressure (AP); AP_{Noise}: noise in AP in terms of the control theory; $AP_{Measured}$: measured AP; $G(f)$: transfer function of the controller; $H(f)$: transfer function from hind-limb electrical stimulation (HES) to the AP response; K_P: proportional gain; K_I: integral gain; f and j denote the frequency and imaginary unit, respectively (see Appendix A for details). (**B**) Functions that convert the HES command into the stimulus current and the stimulus frequency. (**C**) Simulation results showing the feedback control of AP by HES. At time zero, the target AP was set at –20 mmHg. In the simulation, a sinusoidal wave (3 Hz, 15 mmHg in amplitude) was added to mimic the pulse pressure in AP. White lines indicate the 2-s moving averaged data of the simulated AP response.

coherence value became smaller in the frequency range above 0.1 Hz but still retained a value of 0.5, indicating that approximately half of the AP variation was explained by the HES input.

The general feature of the dynamic characteristics of the AP response to HES approximated what is known as a second order low-pass filter with a pure dead time, which is mathematically described as:

$$H(f)=\frac{-K}{1+2\zeta\frac{f}{f_N}j+\left(\frac{f}{f_N}j\right)^2}\exp(-2\pi fjL) \quad (3)$$

where K is the steady-state gain, f_N is the natural frequency, ζ is the damping ratio, and L is the pure dead time. When we performed an iterative non-linear least square fitting using a downhill Simplex method, K, f_N, ζ and L were estimated as 10.2±1.6 mmHg/mA, 0.040±0.004 Hz, 1.80±0.24 and 1.38± 0.13 s, respectively. A model transfer function shown in **Figure 3C** was drawn using K, f_N, ζ and L of 10 mmHg/mA, 0.04 Hz, 2 and 1 s, respectively.

Development of a Feedback Controller

We used a classical feedback controller to adjust the stimulus intensity of HES[23–25] In reference to **Figure 4A**, a HES command is determined based on a difference between measured and target AP values. $G(f)$ represents the transfer function of the controller with a proportional gain (K_P) and an integral gain (K_I). $H(f)$ indicates the model transfer function shown in **Figure 3C**. A detailed mathematical description of the controller is supplied in Appendix A.

To circumvent a threshold phenomenon in the stimulus current-AP response relationship (see Appendix B for details), the HES command (in an arbitrary unit) was transformed into the stimulus current (in mA) by a factor of 1 (**Figure 4B, Left**) only when the HES command exceeded unity. When the HES command was less than unity, the stimulus current was held at 1 mA and the HES command was transformed into the stimulus frequency (in Hz) by a factor of 10 (**Figure 4B, Right**). The stimulation was turned off when the HES command became negative.

Several sets of simulations were conducted using the model transfer function. The target AP was set at 20 mmHg below the baseline AP. To mimic the pulse pressure in AP, a 3-Hz sinusoidal wave (corresponding to the HR of 180 beats/min) with an amplitude of 15 mmHg (corresponding to the pulse pressure of 30 mmHg) was added to the AP signal. To avoid pulsatile variation in the HES command, we set the proportional gain at zero. Under this condition, when the integral gain was set at 0.001, AP decreased gradually and it took more than 3 min to reach the target AP (**Figure 4C, Left**). When the integral gain was set at 0.005, AP decreased more promptly and reached the target AP in less than 1 min (**Figure 4C, Center**). When the integral gain was set at 0.01, the AP response occurred more rapidly but showed significant oscillations before settling (**Figure 4C, Right**). Based on these simulation results, we set the proportional gain at zero and the integral gain at 0.005 for the actual feedback-control experiment in Protocol 4.

Performance of the Feedback Controller

Figure 5A demonstrates the AP regulation by HES obtained from 2 typical animals. The proportional and integral gains of the controller were not altered among the animals (ie, K_P=0, K_I=0.005). The white line in the AP trace indicates 2-s moving averaged data. The target AP was set at 20 mmHg below the AP value just before the application of HES. The feedback controller was activated for 10 min, which decreased AP at the target level. The HES command was individualized via the feedback mechanism. In the left panel of **Figure 5A**, the HES command gradually increased throughout the 10-min regulation. In the right panel of **Figure 5A**, the HES command was less than unity

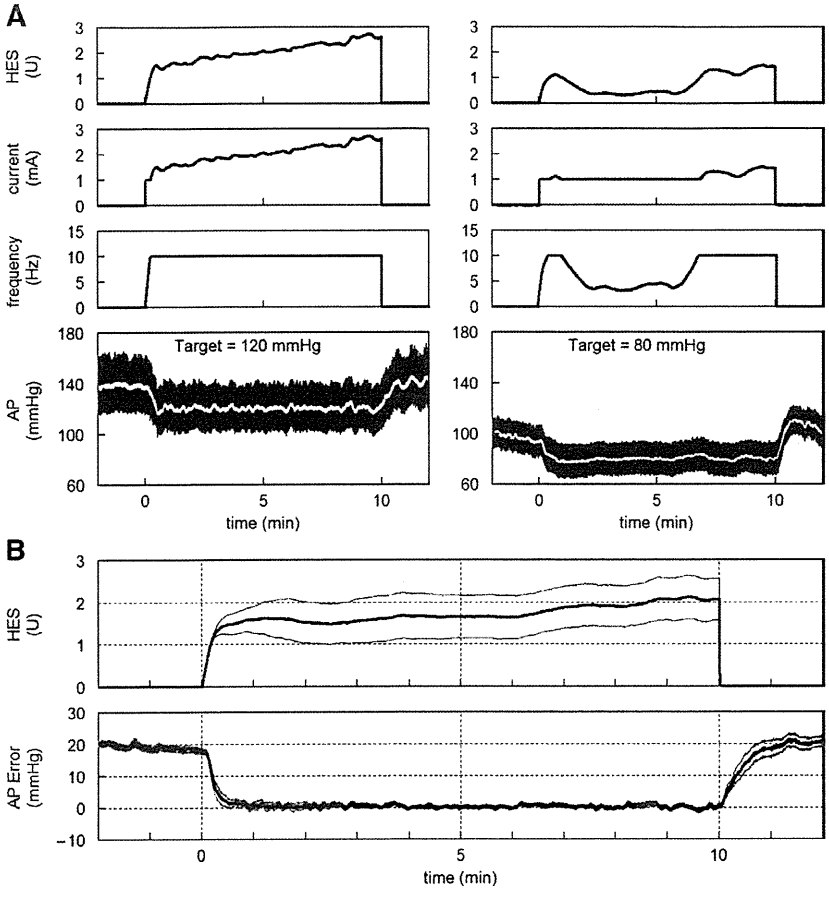

Figure 5. (**A**) Results of 10-min feedback control of arterial pressure (AP) by hind-limb electrical stimulation (HES) obtained from 2 cats. In each cat, the target AP was set at 20 mmHg below the baseline AP value. The current and frequency of HES were automatically adjusted to keep the AP at the target level. (**B**) HES command and the error signal between the target AP and measured AP averaged from 8 cats. The thick and thin lines indicate mean ± SE values, respectively.

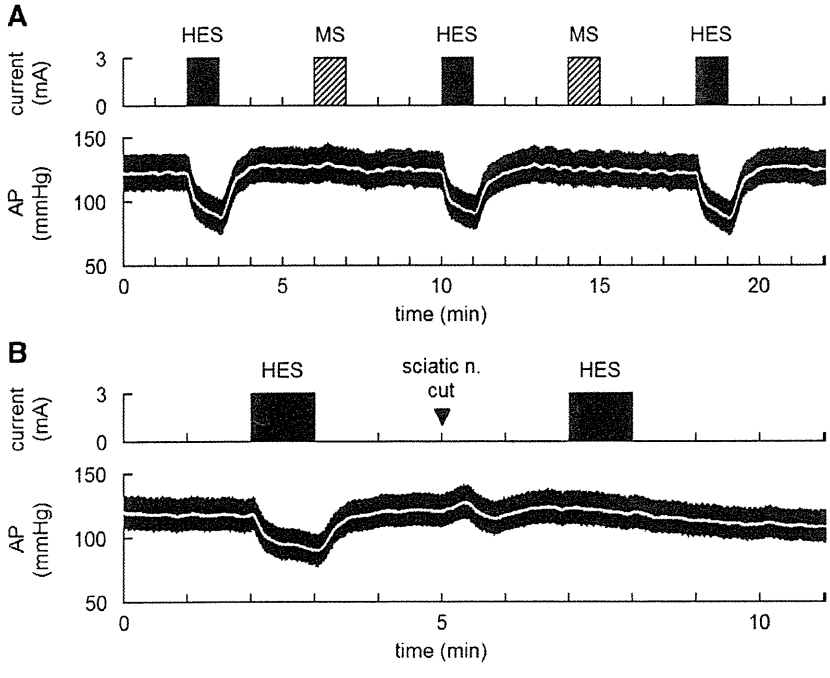

Figure 6. (**A**) Effects of electrical stimulation of the triceps surae muscle (MS) in comparison to hind-limb electrical stimulation (HES). Although muscle twitching was observed, there was no change in arterial pressure (AP) during MS. (**B**) Effects of sectioning the ipsilateral sciatic nerve on the HES-induced changes in AP. After the severance of the ipsilateral sciatic nerve, HES no longer produced significant hypotension.

from 1 to 7 min of the 10-min regulation. In this time period, the HES command altered the stimulus frequency rather than the stimulus current.

Mean and mean ± SE values of the HES command averaged from 8 animals are shown in the top panel of **Figure 5B**. There was a large variance in the HES command among the animals, suggesting inter-individual differences in the responsiveness to HES. The target AP was 102.5±5.6 mmHg across the animals. The error signal between the target AP and measured AP disappeared in less than 1 min (**Figure 5B**,

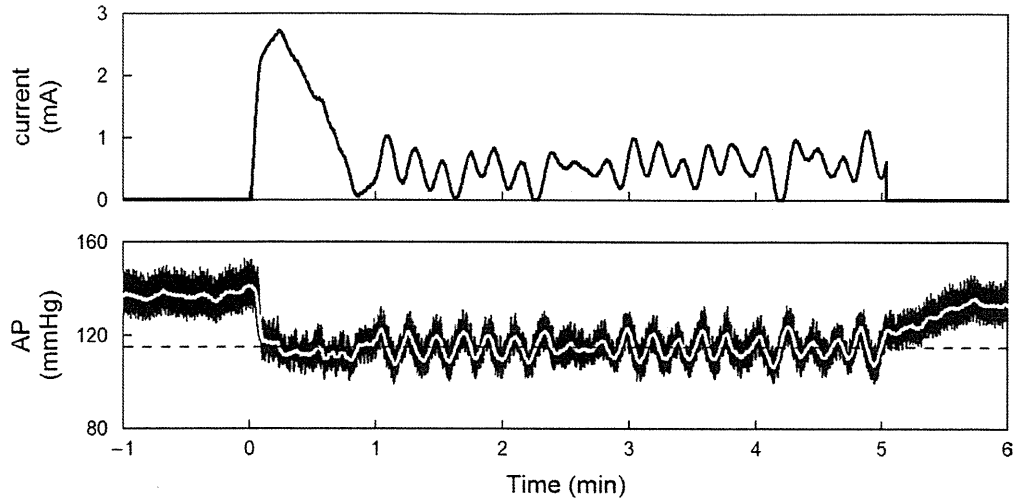

Figure 7. Typical recordings showing failure of controlling the intensity of the hind-limb electrical stimulation during the course of controller development. In this experimental run, only the stimulus current was controlled with a fixed stimulus frequency at 10 Hz. The controller showed on–off type controller behavior once the arterial pressure (AP) approached the target level. The horizontal dashed line indicates the target AP level.

Bottom). The time required for the AP response to reach 90% of the target AP decrease was 38±10 s. Thereafter, the error remained very small until the end of the 10-min regulation. The standard deviation of the steady-state error was 1.3±0.1 mmHg. After the end of the feedback regulation, the error signal gradually returned to approximately 20 mmHg.

Figure 6 represents typical results of the supplemental protocols. Electrical stimulation of the triceps surae muscle (denoted as "MS") did not change AP significantly in spite of visible twitching of the stimulated muscle, suggesting that the depressor response to HES was not the outcome of the direct muscle stimulation (**Figure 6A**). Sectioning the ipsilateral sciatic nerve abolished the depressor effect of HES, suggesting that somatic afferent signals were delivered through the sciatic nerve to the central nervous system during HES (**Figure 6B**).

Discussion

We identified the dynamic input–output relationship between HES and the AP response. By using the model transfer function from HES to AP, we were able to develop a servo-controller that automatically adjusted the HES command to reduce AP at a prescribed target level.

Development of the Feedback Controller

The stimulus current-AP response relationship showed a monotonous decreasing slope (**Figure 2C**). Because the effect of the pulse width was statistically insignificant, we chose the stimulus current as a primary control variable. The problem with using the stimulus current for the control variable was that a certain threshold current existed between 0 and 1 mA where the AP response to HES became discontinuous. If the stimulus current happened to be feedback controlled near the threshold current, AP showed significant oscillation around the target level (**Figure 7**, see Appendix B for details). To avoid such a problem related to the threshold current, we set the minimum current to 1 mA (above the threshold current) and used the stimulus frequency as a secondary control variable (**Figure 4B**).

The stimulus frequency-AP response relationship revealed a valley-shaped curve with the nadir of approximately 10 Hz (**Figure 2D**). The result is similar to that obtained by stimulating hamstring muscle afferent nerves[26] From the viewpoint of controller design, the valley-shaped input–output relationship is troublesome because the proportional-integral controller only assumes a monotonous input–output relationship[23] To avoid the problem of the valley-shaped input–output relationship, we limited the stimulus frequency to the range from 0 to 10 Hz (**Figure 4B, Right**). A similar strategy of selecting the monotonous input–output portion was used in a previous study[12]

We quantified the dynamic AP response to HES using a transfer function analysis (**Figure 3B**), and modeled it by a second-order low-pass filter with a pure dead time (**Figure 3C**). Once the transfer function is modeled, we could construct a numerical simulator for the feedback controller design (**Figure 4A**). Because the optimization of control parameters usually requires a number of trials, even if the initial values are selected via classical methods such as the Ziegler–Nichols' method[23] it is impractical to determine optimal parameter values without using the simulator. The simulation results indicated that the integral gain value of 0.005 would provide rapid and stable AP regulation (**Figure 4C**). Because the controller was designed via intensive simulations, AP was actually controlled at the target level with a small variance (**Figure 5B, Bottom**). Note that the current and frequency of HES were automatically adjusted and individualized via the feedback mechanism (**Figure 5A**).

Bionic Strategies Using Neural Interfaces

A framework of treating cardiovascular diseases using neural interfaces is intriguing because the autonomic nervous system exerts powerful influences on the circulatory system. In previous studies, we identified the dynamic characteristics of the arterial baroreflex system and used them to design an artificial vasomotor center. The artificial vasomotor center was able to control AP by stimulating the celiac ganglia in anesthetized rats[10,11] or the spinal cord in anesthetized cats[12] The strength and rapidity of the neural effect on the cardiovascular system compared with that of the

humoral effect[27,28] make the neural interventions desirable for the rapid and stable restoration of AP against acute disturbances such as those induced by postural changes. Gotoh et al demonstrated that a direct neural interface to the rostral ventrolateral medulla also enabled rapid and stable restoration of AP during nitroprusside-induced hypotension in conscious rats?[29] The bionic system to control AP has also been applied in human subjects![13]

Although the aforementioned bionic systems aimed to maintain AP against acute hypotension by increasing sympathetic nerve activity;[10–13,29] sympathoinhibition might also be required for the treatment of cardiovascular diseases accompanying sympathetic overactivity. Baroreceptor activation is one of the potential sympathoinhibitory neural modulation?[8,9] In the present study we only demonstrated a framework of short-term AP control by HES. With a development of proper implanting electrodes, however, we might be able to control AP chronically using HES. Although carotid sinus baroreceptor stimulation has a potential to treat drug-resistant hypertension? it could activate peripheral chemoreflex by stimulating carotid bodies. HES might circumvent such unintentional chemoreflex activation. Another clinical implication will be the treatment of chronic heart failure. Although the vagal effect of HES was not evaluated in the present study, acupuncture stimulation might facilitate cardiac vagal activity?[30] Because chronic intermittent vagal nerve stimulation increased the survival of chronic heart failure rats?[7] chronic intermittent HES might be used as an alternative method of direct vagal nerve stimulation for the treatment of chronic heart failure.

Study Limitations

First, we did not identify the mechanism of HES. Because sectioning of the ipsilateral sciatic nerve abolished the AP response to HES (**Figure 6B**), somatic afferent is involved in the effect of HES. In a series of studies, Chao et al and Li et al demonstrated that electroacupuncture activated group III and IV fibers in the median nerves and inhibited sympathetic outflow via activation of μ- and δ-opioid receptors in the rostral ventrolateral medulla?[31,32] Whether a similar mechanism underlies in the rapid-onset and short-lasting effect of HES awaits further studies.

Second, we used pentobarbital anesthesia. Although peripheral neurotransmissions of norepinephrine and acetylcholine can be assessed under the same anesthesia;[28,33] because pentobarbital can suppress many neurotransmitters in the central nervous system;[34] anesthesia might compromise the HES effect. Further studies are required to establish the utility of HES in awake conditions.

Third, we set the proportional gain of the controller at zero to avoid pulsatile changes in the HES command. However, other approaches such as that using a low-passed signal of measured AP as a controlled variable might also be effective to avoid the pulsatile variation in the HES command.

Finally, a development of implanting electrodes is the prerequisite for chronic use of HES. Intramuscular electrodes used in functional electrical stimulation might be used for HES but further refinements are clearly needed regarding the positioning of electrodes including the depth of implantation?[35,36]

In conclusion, we identified the dynamic characteristics of the AP response to acupuncture-like HES and demonstrated that a servo-controlled HES system was able to reduce AP at a prescribed target level. Although further studies are required to identify the mechanism of HES to reduce AP, acupuncture-like HES would be an additional modality to exert a quantitative depressor effect on the cardiovascular system.

Acknowledgments

This study was supported by the following Grants: "Health and Labour Sciences Research Grant for Research on Advanced Medical Technology", "Health and Labour Sciences Research Grant for Research on Medical Devices for Analyzing, Supporting and Substituting the Function of Human Body", "Health and Labour Sciences Research Grant (H18-Iryo-Ippan-023) (H18-Nano-Ippan-003) (H19-Nano-Ippan-009)", from the Ministry of Health, Labour and Welfare of Japan, and the "Industrial Technology Research Grant Program" from New Energy and Industrial Technology Development Organization of Japan.

References

1. Bilgutay AM, Bilgutay IM, Merkel FK, Lillehei CW. Vagal tuning: A new concept in the treatment of supraventricular arrhythmias, angina pectoris, and heart failure. *J Thorac Cardiovasc Surg* 1968; **56:** 71–82.
2. Braunwald E, Epstein SE, Glick G, Wechsler AS, Braunwald NS. Relief of angina pectoris by electrical stimulation of the carotid-sinus nerves. *N Engl J Med* 1967; **277:** 1278–1283.
3. Schwartz SI, Griffith LS, Neistadt A, Hagfors N. Chronic carotid sinus nerve stimulation in the treatment of essential hypertension. *Am J Surg* 1967; **114:** 5–15.
4. Vanoli E, De Ferrari GM, Stramba-Badiale M, Hull SS Jr, Foreman RD, Schwartz PJ. Vagal stimulation and prevention of sudden death in conscious dogs with a healed myocardial infarction. *Circ Res* 1991; **68:** 1471–1481.
5. Yang JL, Chen GY, Kuo CD. Comparison of effect of 5 recumbent positions on autonomic nervous modulation in patients with coronary artery disease. *Circ J* 2008; **72:** 902–908.
6. Baba R, Koketsu M, Nagashima M, Inasaka H, Yoshinaga M, Yokota M. Adolescent obesity adversely affects blood pressure and resting heart rate. *Circ J* 2007; **71:** 722–726.
7. Li M, Zheng C, Sato T, Kawada T, Sugimachi M, Sunagawa K. Vagal nerve stimulation markedly improves long-term survival after chronic heart failure in rats. *Circulation* 2004; **109:** 120–124.
8. Zucker IH, Hackley JF, Cornish KG, Hiser BA, Anderson NR, Kieval R, et al. Chronic baroreceptor activation enhances survival in dogs with pacing-induced heart failure. *Hypertension* 2007; **50:** 904–910.
9. Mohaupt MG, Schmidli J, Luft FC. Management of uncontrollable hypertension with a carotid sinus stimulation device. *Hypertension* 2007; **50:** 825–828.
10. Sato T, Kawada T, Shishido T, Sugimachi M, Alexander J Jr, Sunagawa K. Novel therapeutic strategy against central baroreflex failure: A bionic baroreflex system. *Circulation* 1999; **100:** 299–304.
11. Sato T, Kawada T, Sugimachi M, Sunagawa K. Bionic technology revitalizes native baroreflex function in rats with baroreflex failure. *Circulation* 2002; **106:** 730–734.
12. Yanagiya Y, Sato T, Kawada T, Inagaki M, Tatewaki T, Zheng C, et al. Bionic epidural stimulation restores arterial pressure regulation during orthostasis. *J Appl Physiol* 2004; **97:** 984–990.
13. Yamasaki F, Ushida T, Yokoyama T, Ando M, Yamashita K, Sato T. Artificial baroreflex: Clinical application of a bionic baroreflex system. *Circulation* 2006; **113:** 634–639.
14. Li P, Pitsillides KF, Rendig SV, Pan HL, Longhurst JC. Reversal of reflex-induced myocardial ischemia by median nerve stimulation: A feline model of electroacupuncture. *Circulation* 1998; **97:** 1186–1194.
15. Longhurst JC. Electroacupuncture treatment of arrhythmias in myocardial ischemia. *Am J Physiol Heart Circ Physiol* 2007; **292:** H2032–H2034.
16. Lujan HL, Kramer VJ, DiCarlo SE. Electroacupuncture decreases the susceptibility to ventricular tachycardia in conscious rats by reducing cardiac metabolic demand. *Am J Physiol Heart Circ Physiol* 2007; **292:** H2550–H2555.
17. Ohsawa H, Okada K, Nishijo K, Sato Y. Neural mechanism of depressor responses of arterial pressure elicited by acupuncture-like stimulation to a hindlimb in anesthetized rats. *J Auton Nerv Syst* 1995; **51:** 27–35.
18. Uchida S, Shimura M, Ohsawa H, Suzuki A. Neural mechanism of bradycardiac responses elicited by acupuncture-like stimulation to a hind limb in anesthetized rats. *J Physiol Sci* 2007; **57:** 377–382.
19. Michikami D, Kamiya A, Kawada T, Inagaki M, Shishido T, Yamamoto K, et al. Short-term electroacupuncture at Zusanli resets the arterial baroreflex neural arc toward lower sympathetic nerve

activity. *Am J Physiol Heart Circ Physiol* 2006; **291:** H318–H326.
20. Yamamoto H, Kawada T, Kamiya A, Kita T, Sugimachi M. Electroacupuncture changes the relationship between cardiac and renal sympathetic nerve activities in anesthetized cats. *Auton Neurosci: Basic and Clinical* 2008; **144:** 43–49.
21. Marmarelis PZ, Marmarelis VZ. Analysis of Physiological Systems. The white noise method in system identification. New York: Plenum; 1978.
22. Snedecor GW, Cochran WG. Statistical Methods, 8th ed. Ames, Iowa: University Press; 1989.
23. Åström K, Hägglund T. PID Controllers: Theory, Design, and Tuning, 2nd ed. City of Publication: Instrument Society of America; 1995.
24. Kawada T, Sunagawa G, Takaki H, Shishido T, Miyano H, Miyashita H, et al. Development of a servo-controller of heart rate using a treadmill. *Jpn Circ J* 1999; **63:** 945–950.
25. Kawada T, Ikeda Y, Takaki H, Sugimachi M, Kawaguchi O, Shishido T, et al. Development of a servo-controller of heart rate using a cycle ergometer. *Heart Vessels* 1999; **14:** 177–184.
26. Johansson B. Circulatory responses to stimulation of somatic afferents with special reference to depressor effects from muscle nerves. *Acta Physiol Scand* 1962; **Suppl 198:** 1–91.
27. Kawada T, Miyamoto T, Miyoshi Y, Yamaguchi S, Tanabe Y, Kamiya A, et al. Sympathetic neural regulation of heart rate is robust against high plasma catecholamines. *J Physiol Sci* 2006; **56:** 235–245.
28. Kawada T, Yamazaki T, Akiyama T, Shishido T, Miyano H, Sato T, et al. Interstitial norepinephrine level by cardiac microdialysis correlates with ventricular contractility. *Am J Physiol Heart Circ Physiol* 1997; **273:** H1107–H1112.
29. Gotoh TM, Tanaka K, Morita H. Controlling arterial blood pressure using a computer-brain interface. *Neuroreport* 2005; **16:** 343–347.
30. Nishijo K, Mori H, Yosikawa K, Yazawa K. Decreased heart rate by acupuncture stimulation in humans via facilitation of cardiac vagal activity and suppression of cardiac sympathetic nerve. *Neurosci Lett* 1997; **227:** 165–168.
31. Chao DM, Shen LL, Tjen-A-Looi S, Pitsillides KF, Li P, Longhurst JC. Naloxone reverses inhibitory effect of electroacupuncture on sympathetic cardiovascular reflex responses. *Am J Physiol Heart Circ Physiol* 1999; **276:** H2127–H2134.
32. Li P, Tjen-A-Looi SC, Longhurst JC. Rostral ventrolateral medullary opioid receptor subtypes in the inhibitory effect of electroacupuncture on reflex autonomic response in cats. *Auton Neurosci: Basic and Clinical* 2001; **89:** 38–47.
33. Kawada T, Yamazaki T, Akiyama T, Li M, Ariumi H, Mori H, et al. Vagal stimulation suppresses ischemia-induced myocardial interstitial norepinephrine release. *Life Sci* 2006; **78:** 882–887.
34. Adachi YU, Yamada S, Satomoto M, Watanabe K, Higuchi H, Kazama T. et al. Pentobarbital inhibits L-DOPA-induced dopamine increases in the rat striatum: An in vivo microdialysis study. *Brain Res Bull* 2006; **69:** 593–596.
35. Guevremont L, Norton JA, Mushahwar VK. Physiologically based controller for generating overground locomotion using functional electrical stimulation. *J Neurophysiol* 2007; **97:** 2499–2510.
36. Hardin E, Kobetic R, Murray L, Corado-Ahmed M, Pinault G, Sakai J, et al. Walking after incomplete spinal cord injury using an implanted FES system: A case report. *J Rehabil Res Dev* 2007; **44:** 333–346.

Appendix A

Framework of the Feedback Controller

Figure 4A is a simplified block diagram of the feedback controller system used in the present study. The controller was based on a proportional-integral controller[23–25] $G(f)$ represents the transfer function of the controller.

$$G(f)=-K_P+\frac{-K_I}{2\pi fj} \quad \text{(A1)}$$

where K_P and K_I denote proportional and integral gains, respectively. j represents the imaginary unit. Negative signs for the proportional and integral gains compensate for the negative input–output relationship between HES and the AP response. $H(f)$ represents a model transfer function from HES to AP determined from Protocol 3. The measured AP can be expressed as:

$$AP_{Measured}(f)=H(f)HES(f)+AP_{Noise}(f) \quad \text{(A2)}$$

where $AP_{Noise}(f)$ is the AP fluctuation such as that associated with changes in animal conditions. The controller compares the measured AP with the target AP, and adjusts the HES command to minimize the difference between them according to the following equation:

$$HES(f)=G(f)[AP_{Target}(f)-AP_{Measured}(f)] \quad \text{(A3)}$$

By eliminating $HES(f)$ from the equations A2 and A3, the overall controller characteristics are described as:

$$AP_{Measured}(f)=\frac{G(f)H(f)}{1+G(f)H(f)}AP_{Target}(f)+\frac{1}{1+G(f)H(f)}AP_{Noise}(f) \quad \text{(A4)}$$

The equation A4 indicates that if $G(f)$ is properly selected so that $G(f)H(f)$ becomes by far greater than unity, the measured AP approaches the target AP whereas the noise term is significantly attenuated over the frequency range of interest.

Appendix B

Problem with the Threshold Current

We tried to adjust the intensity of HES by the stimulus current alone. When the stimulus current happened to be feedback controlled near a threshold current, however, the controller showed an on–off type controller behavior around the target AP level, as shown in **Figure 7**. At time zero, the controller was activated. The stimulus current increased to approximately 2.7 mA in the beginning and then decreased to a value below 1 mA, accompanying the AP reduction around a target level (a horizontal dashed line). However, the stimulus current and AP did not stabilize. Because the AP response was discontinuous at the threshold current (ie, the depressor effect of HES was abruptly turned on and off), the controller could not adjust the stimulus current in a continuous manner. To avoid this kind of on–off type controller behavior, we introduced the stimulus frequency as the secondary control variable (**Figure 4B**).

J Artif Organs (2009) 12:17–22
DOI 10.1007/s10047-008-0438-z

MINIREVIEW

Toru Kawada, MD, PhD · Masaru Sugimachi, MD, PhD

Artificial neural interfaces for bionic cardiovascular treatments

Abstract An artificial nerve, in the broad sense, may be conceptualized as a physical and logical interface system that reestablishes the information traffic between the central nervous system and peripheral organs. Studies on artificial nerves targeting the autonomic nervous system are in progress to explore new treatment strategies for several cardiovascular diseases. In this article, we will review our research targeting the autonomic nervous system to treat cardiovascular diseases. First, we identified the rule for decoding native sympathetic nerve activity into a heart rate using transfer function analysis, and established a framework for a neurally regulated cardiac pacemaker. Second, we designed a bionic baroreflex system to restore the baroreflex buffering function using electrical stimulation of the celiac ganglion in a rat model of orthostatic hypotension. Third, based on the hypothesis that autonomic imbalance aggravates chronic heart failure, we implanted a neural interface into the right vagal nerve and demonstrated that intermittent vagal stimulation significantly improved the survival rate in rats with chronic heart failure following myocardial infarction. Although several practical problems need to be resolved, such as those relating to the development of electrodes feasible for long-term nerve activity recording, studies of artificial neural interfaces with the autonomic nervous system have great possibilities in the field of cardiovascular treatment. We expect further development of artificial neural interfaces as novel strategies to cope with cardiovascular diseases resistant to conventional therapeutics.

Received: June 24, 2008

T. Kawada (✉) · M. Sugimachi
Department of Cardiovascular Dynamics, Advanced Medical Engineering Center, National Cardiovascular Center Research Institute, Osaka 565-8565, Japan
Tel. +81-6-6833-5012; Fax +81-6-6835-5403
e-mail: torukawa@res.ncvc.go.jp

Part of this article is a translation of an article in Japanese that appeared in *Jinkozoki* 2006;3(3):352–355

Key words Autonomic nervous system · Arterial pressure · Orthostatic hypotension · Heart failure · Transfer function

Introduction

Peripheral nerves are the pathways that convey information from peripheral organs to the central nervous system and commands from the central nervous system to peripheral organs. Damage to the peripheral nerves caused by injury or disease is disadvantageous to living organs. In the narrow sense, an artificial nerve would indicate a replacement of the nerve fiber or nerve bundle with artificial materials capable of conducting nerve impulses. In the broad sense, the artificial nerve may be conceptualized as a physical and logical interface system that reestablishes the information traffic between the central nervous system and peripheral organs. Studies on artificial eyes and ears aim to restore sensory functions by building neural interfaces between artificial sensory devices and sensory nerves, the brainstem, or the sensory cortex.[1–4] Studies on functional electrical stimulation aim to restore motor functions via electrical activation of lower motor neurons through stimulation of axons in peripheral nerves or within the spinal cord.[5] Functional electrical stimulation may also be applied directly to skeletal muscles.[6] In addition to these studies on artificial nerves relating to the sensory and motor systems, studies targeting the autonomic nervous system are in progress to explore new treatment strategies for cardiovascular diseases.

The heart has automaticity, which allows it to continue beating even in the absence of regulation by the autonomic nervous system. Loss of autonomic nervous regulation does not instantly terminate the circulation. In this sense, the significance of studies on artificial nerves targeting the autonomic nervous system to treat cardiovascular diseases may be somewhat elusive compared with studies related to the sensory and motor systems. However, the disruption of the autonomic nervous regulation critically affects the activities

of daily living. As an example, patients with severe orthostatic hypotension cannot maintain adequate arterial pressure to remain conscious during sitting or in the standing position and are forced to become bedridden. An artificial neural interface with the autonomic nervous system is expected to be an effective countermeasure to such diseased conditions. In this article, we will review our research targeting the autonomic nervous system to treat cardiovascular diseases.

Neurally regulated cardiac pacemaker

Regulatory systems in living organs, such as the autonomic nervous system, sense multiple physiological variables and control the effector organs accordingly. The first requirement in the development of an artificial neural interface system that can control effector organs is to decode native neural impulses quantitatively and interpret the commands from the central nervous system to the effector organs. In reference to the sympathetic heart rate control mechanism, although sympathetic activation is known to increase heart rate, a qualitative understanding of the input–output relationship is of little use in the development of a neurally regulated cardiac pacemaker. To examine the input–output relationship between these two variables, we measured left cardiac sympathetic nerve activity and heart rate in anesthetized rabbits.[7] The cervical vagal nerves were sectioned to avoid any vagal effects on heart rate. By imposing random pressure variations on the isolated carotid sinuses, we perturbed sympathetic nerve activity via the carotid sinus baroreflex. Plotting the instantaneous heart rate versus sympathetic nerve activity did not reveal any apparent correlations between the two signals (Fig. 1A). This is because the current heart rate is not determined solely by current sympathetic nerve activity but is also influenced by the past history of sympathetic nerve activity.

To identify the dynamic input–output relationship between sympathetic nerve activity and heart rate, including the effect of past history, we employed a white noise analysis used in the engineering field (see Appendix A for details). The transfer function from sympathetic nerve activity to heart rate approximated a low-pass filter (Fig. 1B). The response of the heart rate became smaller and more delayed as the frequency of input perturbation increased. Berger et al. identified similar low-pass-filterlike characteristics of sympathetic heart rate control using random electrical stimulation of the cardiac sympathetic nerve in anesthetized dogs.[8] When we calculated the impulse response via the inverse Fourier transform of the transfer function (see Appendix A for details), the impulse response revealed a significant positive value for approximately 10 s. This result indicates that sympathetic nerve activity at any given time influences heart rate for approximately 10 s in rabbits (Fig. 1B). Once the impulse response is obtained, we can predict the output signal (heart rate) from the convolution integral between the input signal (sympathetic nerve activity) and the impulse response. The heart rate predicted from the measured sympathetic nerve activity demonstrated good agreement with the measured heart rate (Fig. 1C). Although several practical problems need to be resolved, accurate prediction of the instantaneous heart rate makes the transfer function approach extremely attractive as a principle for designing a neurally regulated cardiac pacemaker.

Here we further discuss transfer function analysis to aid in-depth understanding. In the above-mentioned study,[7] we calculated the transfer function from left cardiac sympathetic nerve activity to heart rate. In reality, a branch of the left cardiac sympathetic nerve was sectioned and the nerve activity was recorded from the proximal end of the sectioned nerve. Therefore, the sympathetic nerve from which activity was recorded could not affect heart rate at the time of the experiment. In addition, because the sinus node is predominantly innervated by the right cardiac sympathetic

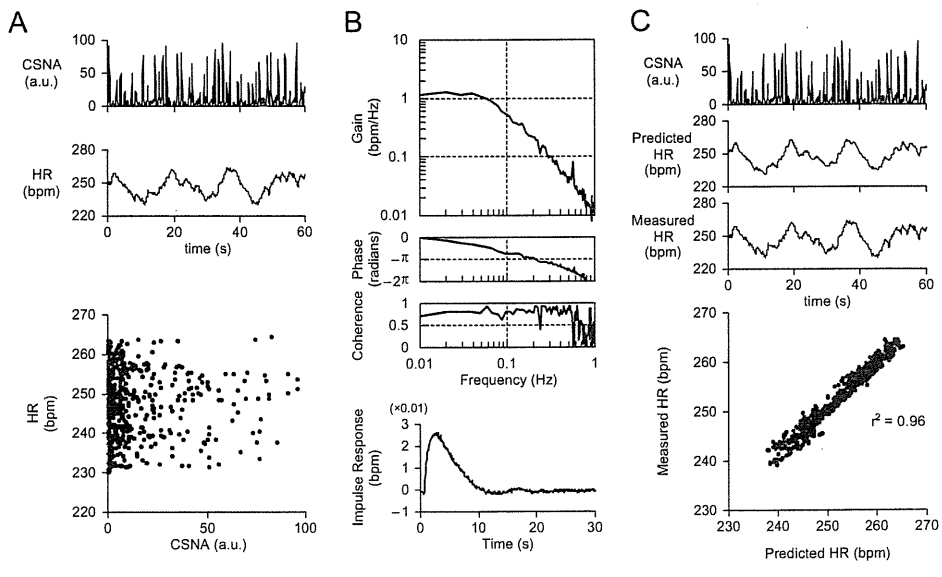

Fig. 1A–C. Decoding of sympathetic heart rate control.[7] **A** Recordings of cardiac sympathetic nerve activity (*CSNA*) and heart rate (*HR*), which were then plotted against each other. **B** Transfer function from CSNA to HR and the corresponding impulse response. **C** Prediction of HR from CSNA using the transfer function. A scatter plot of measured HR versus predicted HR shows the accuracy of this prediction

nerve, changes in heart rate are produced mainly by the right cardiac sympathetic nerve.[9] An implicit assumption of the study is that left cardiac sympathetic nerve activity could be a proxy of the total sympathetic nerve activity that regulates the heart rate. The high coherence between left cardiac sympathetic nerve activity and heart rate is in support of this assumption (Fig. 1B). If the heart rate was regulated by a mechanism totally independent of left cardiac sympathetic nerve activity, the coherence function would have shown values close to zero. We verified our assumption by simultaneously recording left and right cardiac sympathetic nerve activities.[10] There was no apparent laterality of cardiac sympathetic nerve activities in response to dynamic carotid sinus baroreflex perturbation. The laterality observed in the sympathetic effects on the heart rate and ventricular contractility[9] may be mainly attributable to the different distributions of left and right cardiac sympathetic nerves within the heart.

Bionic baroreflex system

Multiple system atrophy (Shy–Drager syndrome) is caused by a disorder of the autonomic nervous system. Shy–Drager patients suffer from severe orthostatic hypotension because of the lack of a baroreflex buffering effect. Although countermeasures to orthostatic hypotension are used, such as administration of pressor agents and volume expansion, these treatments may induce supine hypertension. Ideal treatment would increase arterial pressure only when necessary, i.e., a position-dependent, or more accurately a pressure-dependent, pressor effect is required. In Shy–Drager patients, plasma noradrenaline levels are nearly normal in the supine position and increase following tyramine administration, indicating that peripheral postganglionic sympathetic nerves are relatively spared but only weakly activated by postural changes.[11] If we can encode the information necessary for arterial pressure regulation and deliver those signals to the postganglionic sympathetic system, orthostatic hypotension may be prevented using artificial sympathetic neural interventions.

Because a single nerve fiber discharges according to the all-or-nothing principle, it conveys information by frequency modulation. In contrast, multiple-fiber recording of a nerve bundle exhibits both frequency and amplitude modulations. This is because the amplitude of multiple-fiber recording is the weighted sum of concurrently discharging nerve impulses in the nerve bundle. Nerve fibers adjacent to the electrodes will contribute more to the amplitude generation. The ultimate goal of an artificial neural interface would be to create a respective interface with each nerve fiber in the bundle that could reproduce both the frequency and amplitude modulations. It is unrealistic at present, however, to establish such a complete interface, given the large number of nerve fibers and the small size of the interface.

An alternative strategy for neural interventions is to create a single neural interface to the whole nerve bundle and to treat the system from nerve bundle stimulation to the effector response as a peripheral effector system. Using the electrical stimulation of the celiac ganglion, we explored the development of an artificial vasomotor center to restore normal arterial baroreflex function in rats with central baroreflex failure.[12,13] We first identified the dynamic characteristics of the carotid sinus baroreflex by imposing random pressure perturbations on the isolated carotid sinuses. The transfer function from baroreceptor pressure input to arterial pressure is defined as the native baroreflex function $[H_{Native}(f)]$. Next, we imposed random electrical stimulations on the celiac ganglion and quantified the transfer function from electrical stimulation to the arterial pressure response $[H_{Stim\rightarrow AP}(f)]$. Because the celiac ganglion governs a large abdominal vascular bed, electrical stimulation of the celiac ganglion effectively increased arterial pressure. The transfer function of the controller $[H_{Bionic}(f)]$ was then determined in the frequency domain to fulfill the following equation (Fig. 2A, see Appendix B for details):

$$H_{Bionic}(f)H_{Stim\rightarrow AP}(f) = H_{Native}(f)$$

In a typical experimental result (Fig. 2B), a head-up tilt did not decrease arterial pressure substantially in a rat with a normal baroreflex. In contrast, the same head-up tilt caused significant hypotension in a rat with baroreflex failure. Activation of the bionic baroreflex system was able to restore the baroreflex buffering to a degree similar to that observed in the rat with a normal baroreflex.

Note that native neural discharge of the celiac ganglion was not recorded to develop the bionic baroreflex system,[12,13] whereas recording of the native cardiac sympathetic nerve activity was essential for the development of a neurally regulated cardiac pacemaker.[7] This distinction comes from the fact that the artificial vasomotor center was designed to control the peripheral effector system via electrical stimulation of the celiac ganglion to exert an arterial pressure response. A variety of interventions capable of changing arterial pressure can be treated as a peripheral effector of the bionic baroreflex system. We identified the transfer function from epidural spinal cord stimulation to the arterial pressure response and demonstrated that the bionic baroreflex system using epidural spinal cord stimulation could prevent orthostatic hypotension in anesthetized cats.[14] Yamasaki et al. applied the bionic baroreflex system using epidural spinal cord stimulation to prevent hypotension after sudden deflation of the thigh tourniquet in knee joint surgery.[15] Gotoh et al. demonstrated that an artificial neural interface with the vasomotor center (rostral ventrolateral medulla) provided rapid and precise control of arterial pressure in conscious rats.[16]

Bionic treatment against chronic heart failure

The autonomic nervous system plays an important role in maintaining the circulation under normal physiological conditions. Sympathetic activation and vagal withdrawal during exercise are beneficial to increase cardiac output in response

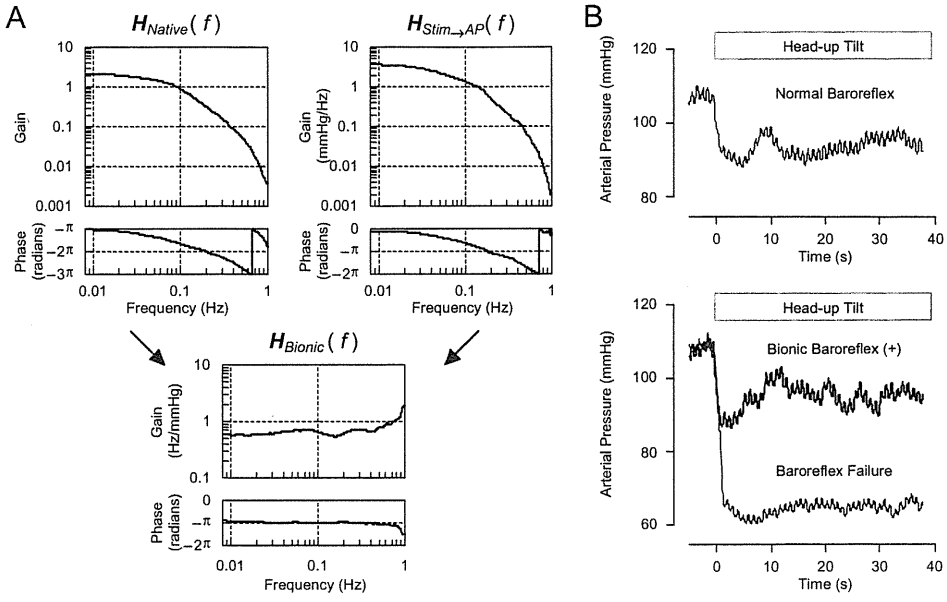

Fig. 2A,B. Arterial pressure regulation by a bionic baroreflex system.[13] **A** Transfer function of the native baroreflex [$H_{Native}(f)$], transfer function from stimulation of the celiac ganglion to arterial pressure [$H_{Stim\rightarrow AP}(f)$], and transfer function of the bionic baroreflex [$H_{Bionic}(f)$]. **B** Arterial pressure responses during a head-up tilt in a rat with normal baroreflex (*top*) and in a rat with central baroreflex failure (*bottom*). Activation of the bionic baroreflex system restored the buffering effect against orthostatic hypotension

to increased oxygen demand. Native autonomic regulation, however, does not always operate properly under disease conditions. Heart failure develops when the heart can no longer provide adequate cardiac output to meet the oxygen demand. While sympathetic activation and vagal withdrawal help compensate for the reduced cardiac performance initially, sympathetic overactivity and vagal withdrawal eventually exacerbate the failing heart, resulting in sympathovagal imbalance and the vicious circle of chronic heart failure. Based on the pathological observation that sympathetic overactivity worsens heart failure, beta-adrenergic blockers and angiotensin converting enzyme inhibitors have been used as treatment. Although beta-blockers were long considered to be contraindicated in heart failure, these drugs were ultimately demonstrated to improve outcome and are now established treatments.[17] Nevertheless, the therapeutic effect of sympathetic blockade is not always sufficient.

We hypothesized that vagal activation would also help terminate the vicious circle in chronic heart failure, and examined whether vagal nerve stimulation could treat chronic heart failure.[18] In halothane-anesthetized rats, the left coronary artery was ligated to produce myocardial infarction. One week later, a telemetry system to record arterial pressure and heart rate and a telestimulator system to stimulate the right vagal nerve were implanted under anesthetized conditions. Another week later (at 14 days after myocardial infarction), surviving rats were divided into vagal stimulation and control groups. In the vagal stimulation group, the right cervical vagal nerve was stimulated intermittently (10-s stimulation per minute) for 6 weeks. The intensity of vagal stimulation was adjusted to decrease the heart rate by 20–30 beats/min. A 140-day follow-up revealed that vagal stimulation significantly increased the survival rate (Fig. 3). Although we did not directly treat the failing heart, the artificial neural interface to the vagal nerve ameliorated heart failure, thereby improved the survival rate.

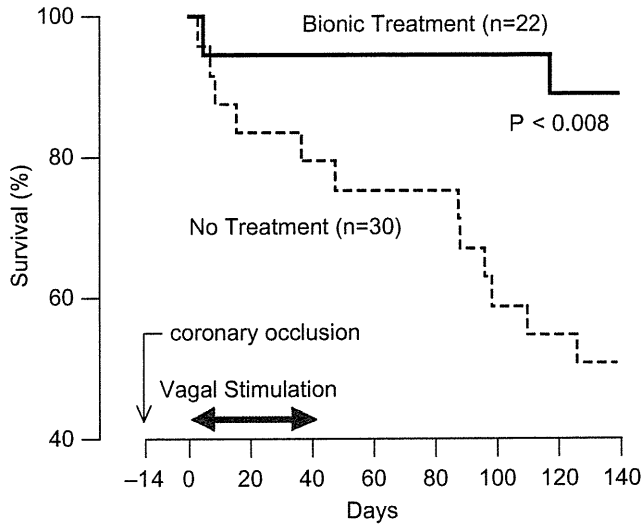

Fig. 3. Survival of rats with chronic heart failure after myocardial infarction.[18] Vagal stimulation dramatically improved the survival rate

The mechanisms by which vagal stimulation ameliorates chronic heart failure are not fully understood. Because vagal stimulation decreases heart rate, myocardial oxygen consumption is reduced. Vagal stimulation can also reduce ventricular contractility via antagonism of the sympathetic effect,[19] which may also help reduce myocardial oxygen demand. Vagal stimulation shows an antifibrillatory effect during ischemic insult in healed myocardial infarction in conscious dogs.[20] In acute myocardial ischemia, vagal stimulation reduces the accumulation of noradrenaline in the myocardial interstitium of the ischemic region.[21] Because catecholamines have cardiotoxicity,[22] reducing myocardial interstitial noradrenaline levels in the ischemic region may be cardioprotective. Vagal stimulation also reduces the

protein levels of endogenous active matrix metalloproteinase-9 during ischemia–reperfusion injury,[23] which may contribute to the inhibition of ventricular remodeling. Because acetylcholine concentrations in the ischemic myocardium are increased via a local releasing mechanism that is independent of voltage-dependent calcium channels,[24,25] vagal stimulation can only induce small additional increases in acetylcholine concentrations in the ischemic region.[21] Given the profound ameliorative effect of vagal stimulation in chronic heart failure,[18] the target of the vagal effect may be the ischemic border zone, rather than the ischemic zone itself. Also, the vagal afferent pathway may modify the central nervous system to exert beneficial effects in chronic heart failure. Development of a new experimental method, such as that using reversible vagal blockade in conscious rats,[26] would help separate the afferent and efferent effects of vagal stimulation. Further studies are required to identify the mechanisms of cardioprotection by vagal stimulation.

Conclusion

In this review, we briefly summarized studies of artificial neural interfaces targeting the autonomic nervous system with the goal of treating several cardiovascular diseases. In all of the studies discussed, creating a logical and physical interface with the autonomic nervous system is the key to effective cardiovascular treatment. In relation to the logical interface, we have demonstrated that the application of white noise analysis was useful in decoding and encoding information for the autonomic nervous system. In relation to the physical interface, electrodes truly capable of long-term recording have not yet been realized. Although we examined the application of sieve-type nerve regeneration electrodes for stimulating and recording the autonomic nerves, further refinements are necessary for practical use. Studies of artificial neural interfaces with the autonomic nervous system are intriguing and have immense possibilities in the field of cardiovascular treatment. We expect further development of artificial neural interfaces as novel strategies to manage cardiovascular diseases that are resistant to conventional therapeutics.

Appendix A

Transfer function analysis

We resampled input–output data of sympathetic nerve activity and heart rate at 10 Hz, and segmented them into eight sets of 50%-overlapping bins of 1024 points each. For each segment, the linear trend was subtracted and a Hanning window was applied. A fast Fourier transform was performed to obtain the frequency spectra of the input and output. Ensemble averages of input power spectra $[S_{XX}(f)]$, output power spectra $[S_{YY}(f)]$, and the cross-spectra between the input and output $[S_{YX}(f)]$ were then calculated. The transfer function was estimated from the following equation:[27]

$$H(f)=\frac{S_{YX}(f)}{S_{XX}(f)} \tag{A1}$$

The coherence function between the input and output was calculated from the following equation:[27]

$$Coh(f)=\frac{|S_{YX}(f)|^2}{S_{XX}(f)S_{YY}(f)} \tag{A2}$$

The coherence function ranges from zero to unity. Zero coherence indicates total independence between the input and output. Unity coherence indicates a perfect linear dependence of the output on the input.

Once the transfer function was identified, we could calculate the impulse response of the system $[h(\tau)]$ via inverse Fourier transform of the transfer function. We then predicted the system response $[y(t)]$ to an input signal $[x(t)]$ from the convolution integral between $h(\tau)$ and $x(t)$ according to the following equation:

$$y(t)=\int_0^T h(\tau)x(t-\tau)d\tau \tag{A3}$$

Although the above convolution integral predicts changes in the output signal in response to changes in the input signal, it cannot usually predict the direct current component or mean value of the output signal. In the case of sympathetic heart rate control, the heart rate does not become zero in the absence of sympathetic stimulation. In the prediction (Fig. 1C), we added the mean value of the measured heart rate to the output signal of the convolution integral to predict the absolute heart rate value.

Appendix B

Designing a bionic baroreflex system

The transfer function of the native baroreflex $[H_{Native}(f)]$ determined the dynamic input–output relationship between baroreceptor pressure input $[P_{Input}(f)]$ and arterial pressure $[AP(f)]$ in the frequency domain:

$$AP(f)=H_{Native}(f)P_{Input}(f) \tag{B1}$$

The transfer function from the stimulus command to the arterial pressure $[H_{Stim\rightarrow AP}(f)]$ determined the dynamic input–output relationship between the stimulus command $[C_{Stim}(f)]$ and arterial pressure in the frequency domain:

$$AP(f)=H_{Stim\rightarrow AP}(f)C_{Stim}(f) \tag{B2}$$

The transfer function of the bionic baroreflex $[H_{Bionic}(f)]$ determined the dynamic input–output relationship between the baroreceptor pressure input and the stimulus command in the frequency domain:

$$C_{Stim}(f)=H_{Bionic}(f)P_{Input}(f) \tag{B3}$$

From equations B2 and B3, arterial pressure regulation by the bionic baroreflex can be described as follows:

$$AP(f) = H_{Stim \rightarrow AP}(f) H_{Bionic}(f) P_{Input}(f) \quad \text{(B4)}$$

Comparison of Eqs. B1 and B4 shows that the bionic baroreflex should fulfill the following equation to reproduce the native baroreflex function:

$$H_{Bionic}(f) = \frac{H_{Native}(f)}{H_{Stim \rightarrow AP}(f)} \quad \text{(B5)}$$

After determining the transfer function of the bionic baroreflex, we obtained the impulse response of the bionic baroreflex system $[h_{Bionic}(\tau)]$ via inverse Fourier transform of the transfer function. We then calculated the stimulus command $[c_{Stim}(t)]$ from the convolution integral between $h_{Bionic}(\tau)$ and the baroreceptor pressure input $[p_{Input}(t)]$, according to the following equation:

$$c_{Stim}(f) = \int_0^T h_{Bionic}(\tau) p_{Input}(t-\tau) d\tau \quad \text{(B6)}$$

In the above convolution integral, $p_{Input}(t)$ was treated as the change in arterial pressure from the arterial pressure value measured immediately before hypotensive intervention.

Acknowledgments This work was supported in part by a Health and Labour Sciences Research Grant for Research on Advanced Medical Technology, a Health and Labour Sciences Research Grant for Research on Medical Devices for Analyzing, Supporting and Substituting the Function of the Human Body, and a Health and Labour Sciences Research Grant from the Ministry of Health, Labour and Welfare of Japan (H18-Iryo-Ippan-023, H19-Nano-Ippan-009).

References

1. Dowling J. Artificial human vision. Expert Rev Med Devices 2005:2:73–85
2. Walter P, Kisvárday ZF, Görtz M, Alteheld N, Rossler G, Stieglitz T, Eysel UT. Cortical activation via an implanted wireless retinal prosthesis. Invest Ophthalmol Vis Sci 2005;46(5):1780–1785
3. Papsin BC, Gordon KA. Cochlear implants for children with severe-to-profound hearing loss. N Engl J Med 2007;357:2380–2387
4. Lim HH, Lenarz T, Joseph G, Battmer RD, Samii A, Samii M, Patrick JF, Lenarz M. Electrical stimulation of the midbrain for hearing restoration: insight into the functional organization of the human central auditory system. J Neurosci 2007;27:13541–13551
5. Mushahwar VK, Jacobs PL, Normann RA, Triolo RJ, Kleitman N. New functional electrical stimulation approaches to standing and walking. J Neural Eng 2007;4(3):S181–S197
6. Sujith OK. Functional electrical stimulation in neurological disorders. Eur J Neurol 2008;15:437–444
7. Ikeda Y, Sugimachi M, Yamasaki T, Kawaguchi O, Shishido T, Kawada T, Alexander J Jr, Sunagawa K. Explorations into development of a neurally regulated cardiac pacemaker. Am J Physiol 1995;269:H2141–H2146
8. Berger RD, Saul JP, Cohen RJ. Transfer function analysis of autonomic regulation. I. Canine atrial rate response. Am J Physiol 1989:256:H142–H152
9. Miyano H, Nakayama Y, Shishido T, Inagaki M, Kawada T, Sato T, Miyashita H, Sugimachi M, Alexander J Jr, Sunagawa K. Dynamic sympathetic regulation of left ventricular contractility studied in the isolated canine heart. Am J Physiol 1998;275: H400–H408
10. Kawada T, Uemura K, Kashihara K, Jin Y, Li M, Zheng C, Sugimachi M, Sunagawa K. Uniformity in dynamic baroreflex regulation of left and right cardiac sympathetic nerve activities. Am J Physiol Regul Integr Comp Physiol 2003;284:R1506–R1512
11. Parikh SM, Diedrich A, Biaggioni I, Robertson D. The nature of the autonomic dysfunction in multiple system atrophy. J Neurol Sci 2002;200:1–10
12. Sato T, Kawada T, Shishido T, Sugimachi M, Alexander J Jr, Sunagawa K. Novel therapeutic strategy against central baroreflex failure: a bionic baroreflex system. Circulation 1999;100:299–304
13. Sato T, Kawada T, Sugimachi M, Sunagawa K. Bionic technology revitalizes native baroreflex function in rats with baroreflex failure. Circulation 2002;106:730–734
14. Yanagiya Y, Sato T, Kawada T, Inagaki M, Tatewaki T, Zheng C, Kamiya A, Takaki H, Sugimachi M, Sunagawa K. Bionic epidural stimulation restores arterial pressure regulation during orthostasis. J Appl Physiol 2004;97:984–990
15. Yamasaki F, Ushida T, Yokoyama T, Ando M, Yamashita K, Sato T. Artificial baroreflex: clinical application of a bionic baroreflex system. Circulation 2006;113:634–639
16. Gotoh TM, Tanaka K, Morita H. Controlling arterial blood pressure using a computer–brain interface. Neuroreport 2005;16: 343–347
17. Mudd JO, Kass DA. Tackling heart failure in the twenty-first century. Nature 2008;451:919–928
18. Li M, Zheng C, Sato T, Kawada T, Sugimachi M, Sunagawa K. Vagal nerve stimulation markedly improves long-term survival after chronic heart failure in rats. Circulation 2004;109:120–124
19. Nakayama Y, Miyano H, Shishido T, Inagaki M, Kawada T, Sugimachi M, Sunagawa K. Heart rate-independent vagal effect on end-systolic elastance of the canine left ventricle under various levels of sympathetic tone. Circulation 2001;104:2277–2279
20. Vanoli E, De Ferrari GM, Stramba-Badiale M, Hull SS Jr, Foreman RD, Schwartz PJ. Vagal stimulation and prevention of sudden death in conscious dogs with a healed myocardial infarction. Circ Res 1991;68:1471–1481
21. Kawada T, Yamazaki T, Akiyama T, Li M, Ariumi H, Mori H, Sunagawa K, Sugimachi M. Vagal stimulation suppresses ischemia-induced myocardial interstitial norepinephrine release. Life Sci 2006;78:882–887
22. Rona G. Catecholamine cardiotoxicity. J Mol Cell Cardiol 1985; 17:291–306
23. Uemura K, Li M, Tsutsumi T, Yamazaki T, Kawada T, Kamiya A, Inagaki M, Sunagawa K, Sugimachi M. Efferent vagal nerve stimulation induces tissue inhibitor of metalloproteinase-1 in myocardial ischemia–reperfusion injury in the rabbit. Am J Physiol Heart Circ Physiol 2007:293:H2254–H2261
24. Kawada T, Yamazaki T, Akiyama T, Sato T, Shishido T, Inagaki M, Takaki H, Sugimachi M, Sunagawa K. Differential acetylcholine release mechanisms in the ischemic and non-ischemic myocardium. J Mol Cell Cardiol 2000:32:405–414
25. Kawada T, Yamazaki T, Akiyama T, Uemura K, Kamiya A, Shishido T, Mori H, Sugimachi M. Effects of Ca^{2+} channel antagonists on nerve stimulation-induced and ischemia-induced myocardial interstitial acetylcholine release in cats. Am J Physiol Heart Circ Physiol 2006;291:H2187–H2191
26. Zheng C, Kawada T, Li M, Sato T, Sunagawa K, Sugimachi M. Reversible vagal blockade in conscious rats using a targeted delivery device. J Neurosci Methods 2006;156:71–75
27. Marmarelis PZ, Marmarelis VZ. Analysis of physiological systems. The white noise method in system identification. New York: Plenum, 1978:131–221

J Physiol Sci (2009) 59:447–455
DOI 10.1007/s12576-009-0055-5

ORIGINAL PAPER

High levels of circulating angiotensin II shift the open-loop baroreflex control of splanchnic sympathetic nerve activity, heart rate and arterial pressure in anesthetized rats

Toru Kawada · Atsunori Kamiya · Meihua Li · Shuji Shimizu · Kazunori Uemura · Hiromi Yamamoto · Masaru Sugimachi

Received: 21 May 2009 / Accepted: 19 July 2009 / Published online: 18 August 2009

Abstract Although an acute arterial pressure (AP) elevation induced by intravenous angiotensin II (ANG II) does not inhibit sympathetic nerve activity (SNA) compared to an equivalent AP elevation induced by phenylephrine, there are conflicting reports as to how circulating ANG II affects the baroreflex control of SNA. Because most studies have estimated the baroreflex function under closed-loop conditions, differences in the rate of input pressure change and the magnitude of pulsatility may have biased the estimation results. We examined the effects of intravenous ANG II (10 μg kg^{-1} h^{-1}) on the open-loop system characteristics of the carotid sinus baroreflex in anesthetized and vagotomized rats. Carotid sinus pressure (CSP) was raised from 60 to 180 mmHg in increments of 20 mmHg every minute, and steady-state responses in systemic AP, splanchnic SNA and heart rate (HR) were analyzed using a four-parameter logistic function. ANG II significantly increased the minimum values of AP (67.6 ± 4.6 vs. 101.4 ± 10.9 mmHg, $P < 0.01$), SNA (33.3 ± 5.4 vs. 56.5 ± 11.5%, $P < 0.05$) and HR (391.1 ± 13.7 vs. 417.4 ± 11.5 beats/min, $P < 0.01$). ANG II, however, did not attenuate the response range for AP (56.2 ± 7.2 vs. 49.7 ± 6.2 mmHg), SNA (69.6 ± 5.7 vs. 78.9 ± 9.1%) or HR (41.7 ± 5.1 vs. 51.2 ± 3.8 beats/min). The maximum gain was not affected for AP (1.57 ± 0.28 vs. 1.20 ± 0.25), SNA (1.94 ± 0.34 vs. 2.04 ± 0.42%/mmHg) or HR (1.11 ± 0.12 vs. 1.28 ± 0.19 beats min^{-1} $mmHg^{-1}$). It is concluded that high levels of circulating ANG II did not attenuate the response range of open-loop carotid sinus baroreflex control for AP, SNA or HR in anesthetized and vagotomized rats.

Keywords Systems analysis · Open-loop gain · Equilibrium diagram · Carotid sinus baroreflex · Rats

T. Kawada (✉) · A. Kamiya · M. Li · S. Shimizu · K. Uemura · M. Sugimachi
Department of Cardiovascular Dynamics, Advanced Medical Engineering Center, National Cardiovascular Center Research Institute, 5-7-1 Fujishirodai, Suita, Osaka 565-8565, Japan
e-mail: torukawa@res.ncvc.go.jp

M. Li · S. Shimizu
Japan Association for the Advancement of Medical Equipment, Tokyo 113-0033, Japan

H. Yamamoto
Division of Cardiology, Department of Internal Medicine, Kinki University School of Medicine, Osaka 589-8511, Japan

Introduction

The arterial baroreflex is an important negative feedback system that stabilizes systemic arterial pressure (AP) during daily activities. The sympathetic arterial baroreflex can be divided into the neural and peripheral arc subsystems [1]. The neural arc characterizes the input–output relation between the baroreceptor pressure input and efferent sympathetic nerve activity (SNA), whereas the peripheral arc defines the input–output relation between SNA and AP. These subsystems operate as a controller and a plant, respectively, in the negative feedback loop. Although the input signal to the neural arc is primarily the absolute input pressure level, the rate of input pressure change [1–3] and the magnitude of pulsatility [4–7] are also important input signals that critically affect the baroreflex function. Many investigators employ pharmacologic interventions, such as intravenous phenylephrine and nitroprusside administration, to estimate baroreflex function under closed-loop conditions. The rate of input pressure change and the

magnitude of pulsatility, however, may vary within and between studies, which could bias the estimation results. In addition, experiments performed under baroreflex closed-loop conditions do not usually permit an evaluation of the baroreflex control of AP, because measured AP cannot be separated into signals for the input pressure and output pressure. An open-loop experiment with isolated baroreceptor regions is therefore required to evaluate the baroreflex function precisely.

Angiotensin II (ANG II) can affect the arterial baroreflex by centrally increasing sympathetic outflow, stimulating sympathetic ganglia and the adrenal medulla, and facilitating neurotransmission at sympathetic nerve endings [8]. Although an acute AP elevation induced by intravenous ANG II does not inhibit SNA compared to an equivalent AP elevation induced by phenylephrine, how circulating ANG II affects the baroreflex control of SNA varies among reports, i.e., intravenous ANG has been shown to attenuate [9, 10] or not attenuate [11, 12] the baroreflex control of SNA. Because it is related to the pathologic sympathoexcitation observed in such cardiovascular diseases as chronic heart failure [13], analyzing the effects of circulating ANG II on the baroreflex open-loop system characteristics will deepen our understanding of the pathologic roles of ANG II. In the present study, we examined the effects of intravenous ANG II (10 μg kg^{-1} h^{-1} or 167 ng kg^{-1} min^{-1}) on the open-loop system characteristics of the baroreflex neural and peripheral arcs in anesthetized rats. We hypothesized that ANG II would increase the minimum SNA and attenuate the range of SNA response because the maximum SNA may be saturated. Contrary to our hypothesis, ANG II increased both the minimum and maximum SNA, preserving the range of SNA response controlled by the arterial baroreflex.

Materials and methods

Animals were cared for in strict accordance with the guiding principles for the care and use of animals in the field of physiological sciences, which has been approved by the Physiological Society of Japan. All experimental protocols were reviewed and approved by the Animal Subjects Committee at the National Cardiovascular Center.

Baroreflex open-loop experiment

Male Sprague–Dawley rats ($n = 8$, 482 ± 14 g body weight, mean ± SE) were anesthetized with an intraperitoneal injection (2 ml/kg) of a mixture of urethane (250 mg/ml) and α-chloralose (40 mg/ml), and mechanically ventilated with oxygen-enriched room air. A venous catheter was inserted into the right femoral vein, and a tenfold dilution of the anesthetic mixture was administered (2 ml kg^{-1} h^{-1}) to maintain an appropriate level of anesthesia. An arterial catheter was inserted into the right femoral artery to measure AP. A cardiotachometer was used to measure heart rate (HR). Another venous catheter was inserted into the left femoral vein to administer Ringer's solution with or without ANG II.

We exposed a postganglionic branch of the splanchnic nerve through a left flank incision and attached a pair of stainless steel wire electrodes (Bioflex wire AS633, Cooner Wire, CA) to record SNA. The nerve and electrodes were covered with silicone glue (Kwik-Sil, World Precision Instruments, Sarasota, FL) for insulation and fixation. To quantify the nerve activity, the preamplified nerve signal was band-pass filtered at 150–1,000 Hz, and then full-wave rectified and low-pass filtered with a cutoff frequency of 30 Hz. Pancuronium bromide (0.4 mg kg^{-1} h^{-1}) was administered to prevent muscular activity from contaminating the SNA recording. At the end of the experiment, we confirmed the disappearance of SNA after an intravenous bolus injection of hexamethonium bromide (60 mg/kg) and recorded the noise level.

The vagal and aortic depressor nerves were sectioned at the neck to avoid reflexes from the cardiopulmonary region and aortic arch. The bilateral carotid sinuses were isolated from the systemic circulation according to previously reported procedures [14, 15]. Briefly, a fine needle with a 7-0 polypropylene suture (PROLENE, Ethicon, GA, USA) was passed through the tissue between the external and internal carotid arteries, and the external carotid artery was ligated close to the carotid bifurcation. The internal carotid artery was embolized using two or three bearing balls (0.8 mm in diameter, Tsubaki Nakashima, Nara, Japan), which were injected from the common carotid artery. The isolated carotid sinuses were filled with warmed Ringer's solution through catheters inserted via the common carotid arteries. Carotid sinus pressure (CSP) was controlled using a servo-controlled piston pump. Heparin sodium (100 U/kg) was given intravenously to prevent blood coagulation. Body temperature was maintained at approximately 38°C with a heating pad.

Protocols

Sympathetic nerve activity and AP responses to CSP perturbations were monitored for at least 30 min after the surgical preparation was completed. If these responses became smaller within this period, the animal was discarded from the study. Possible causes for deteriorations in the responses include surgical damage to the carotid sinus nerves and brain ischemia due to bilateral carotid occlusion.

The CSP was decreased to 60 mmHg for 4–6 min, and then increased every minute from 60 to 180 mmHg using 20-mmHg increments. At least four step cycles were performed under control conditions while Ringer's solution was continuously administered (6 ml kg^{-1} h^{-1}). After recording the control data, the intravenous Ringer's solution was replaced with that containing ANG II (167 ng kg^{-1} min^{-1}). The dose of ANG II was chosen to induce a significant pressor effect based on previous studies [16, 17]. At least three step cycles were performed during ANG II administration.

Data analysis

Data were sampled at 200 Hz using a 16-bit analog-to-digital converter and stored on the hard disk of a dedicated laboratory computer system. To quantify the open-loop static characteristics of the carotid sinus baroreflex, mean values of SNA, AP and HR were calculated during the last 10 s at each CSP level. The effects of ANG II were assessed during the third step cycle after ANG II administration began, at which point the hemodynamic responses to ANG II appeared to reach steady state. Comparisons were made against two control step cycles (control 1 and control 2, see Fig. 1). In each animal, the SNA noise level recorded after the administration of hexamethonium bromide was set to zero. The SNA values obtained at a CSP level of 60 mmHg during control 1 and control 2 were averaged and defined as 100%.

The open-loop characteristics of the AP, SNA and HR responses as functions of CSP were quantified by fitting a four-parameter logistic function to the obtained data as follows [18]:

$$y = \frac{P_1}{1 + \exp[P_2(\mathrm{CSP} - P_3)]} + P_4.$$

where y represents AP, SNA or HR; P_1 is the response range (the difference between the maximum and minimum values of y); P_2 is a slope coefficient; P_3 is the midpoint in CSP; P_4 is the minimum value of y. The maximum gain or maximum slope of the sigmoidal curve was obtained from $P_1P_2/4$.

The open-loop characteristics of the baroreflex peripheral arc (i.e., SNA–AP relation) were quantified using linear regression analysis as follows:

$$\mathrm{AP} = a \times \mathrm{SNA} + b.$$

where a and b represent the slope and intercept of the regression line, respectively.

Statistical analysis

All parameters were compared among control 1, control 2 and ANG II conditions using repeated-measures analysis of variance [19]. When there was a significant difference among the three conditions, all pairwise comparisons were performed using the Student-Neuman-Keuls test. Differences were considered significant at $P < 0.05$. All data are expressed as mean and SE values.

Results

Typical experimental recordings are shown in Fig. 1. The stepwise input from 60 to 180 mmHg was imposed repeatedly on CSP. An increase in CSP decreased SNA. m-SNA represents the 5-s moving-average signal of the percentage of SNA. AP and HR were also decreased in response to increases in CSP. After ANG II administration was initiated, the levels of SNA, AP and HR all increased compared to the levels before ANG II administration. The responses in SNA, AP and HR to the CSP input appeared to be preserved. Data obtained from the three boxes with dashed lines (control 1, control 2 and ANG II) were used for the statistical analysis.

The open-loop characteristics of the total baroreflex revealed sigmoidal nonlinearity (Fig. 2a). No significant differences were observed between the two control conditions. ANG II significantly increased the minimum AP without affecting the response range, slope coefficient or midpoint in CSP (Table 1). The maximum gain of the total baroreflex was unchanged. The open-loop characteristics of the baroreflex control of HR also approximated sigmoidal nonlinearity (Fig. 2b), and no significant differences were observed between the two control conditions. ANG II significantly increased the minimum HR without affecting the response range, slope coefficient or midpoint in CSP (Table 1). The maximum slope of the baroreflex control of HR was unchanged.

The total baroreflex was decomposed into the neural and peripheral arc subsystems. The open-loop characteristics of the baroreflex neural arc revealed sigmoidal nonlinearity (Fig. 3a). There were no significant differences between the two control conditions. ANG II significantly increased the minimum SNA (Table 1). Although the midpoint in CSP was lower in ANG II than in control 1, the difference was not significant when compared with control 2. ANG II did not affect the response range, slope coefficient or the maximum slope of the baroreflex control of SNA. The open-loop characteristics of the baroreflex peripheral arc approximated a straight line (Fig. 3b). There were no significant differences between the two control conditions. ANG II significantly increased the intercept of the regression line (Table 1). AP at 100% SNA did not change significantly, suggesting that the slope of the regression line could be shallower under the ANG II condition. The slope of the

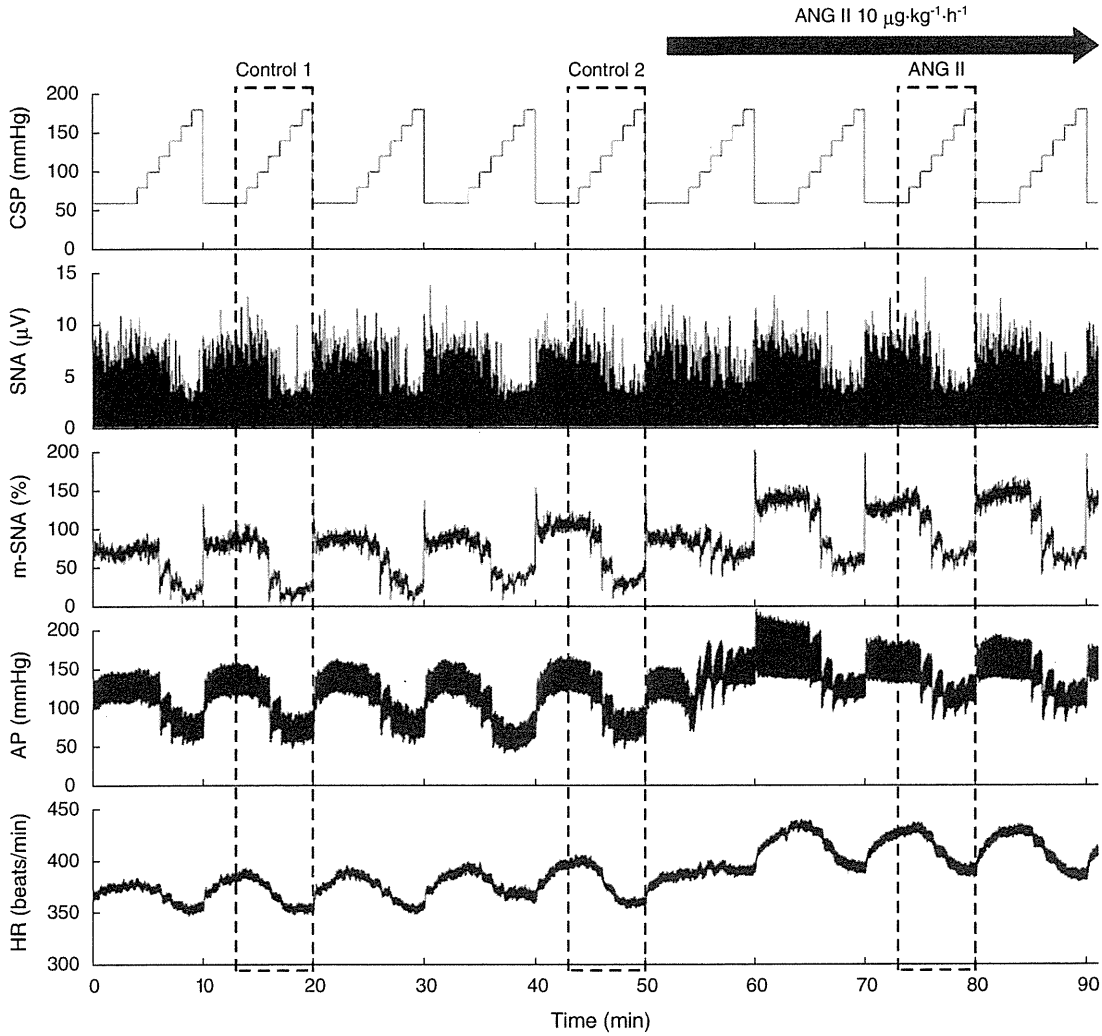

Fig. 1 Typical recordings of carotid sinus pressure (*CSP*), splanchnic sympathetic nerve activity (*SNA*), the 5-s moving-average signal of the percentage of SNA (*m-SNA*), systemic arterial pressure (*AP*) and heart rate (*HR*). CSP was changed stepwise from 60 to 180 mmHg in 20-mmHg increments every minute. Angiotensin II (ANG II) was administered intravenously while the CSP perturbation was continued. ANG II significantly increased SNA, AP and HR. Reflex responses in SNA, AP and HR were not attenuated in the presence of ANG II. *Dashed boxes* indicate the step cycles used for the statistical analysis

regression line, however, was not statistically different among the three conditions.

An equilibrium diagram or a balance diagram was obtained by drawing the neural and peripheral arcs using SNA as the common abscissa and CSP or AP as an ordinate [20–22]. Figure 4 illustrates the equilibrium diagrams under the control 2 (dashed line) and ANG II (solid line) conditions, which were drawn based on the mean parameter values from the logistic function and regression line. Open and filled circles represent the closed-loop operating points under the control 2 and ANG II conditions, respectively. Although AP at the closed-loop operating point was significantly increased by the intravenous ANG II, SNA at the closed-loop operating point was unchanged (Table 1). If ANG II affected the peripheral arc alone, the closed-operating point may have been located at the point depicted by the open triangle. If ANG II affected the neural arc alone, the closed-loop operating point may have been located at the point depicted by the filled triangle.

Discussion

Effects of ANG II on open-loop baroreflex control of SNA

Intravenous ANG II at 167 ng kg^{-1} min^{-1} shifted the open-loop baroreflex control of splanchnic SNA toward higher SNA values without attenuating the size of the response range (Fig. 3a; Table 1). The maximum slope was

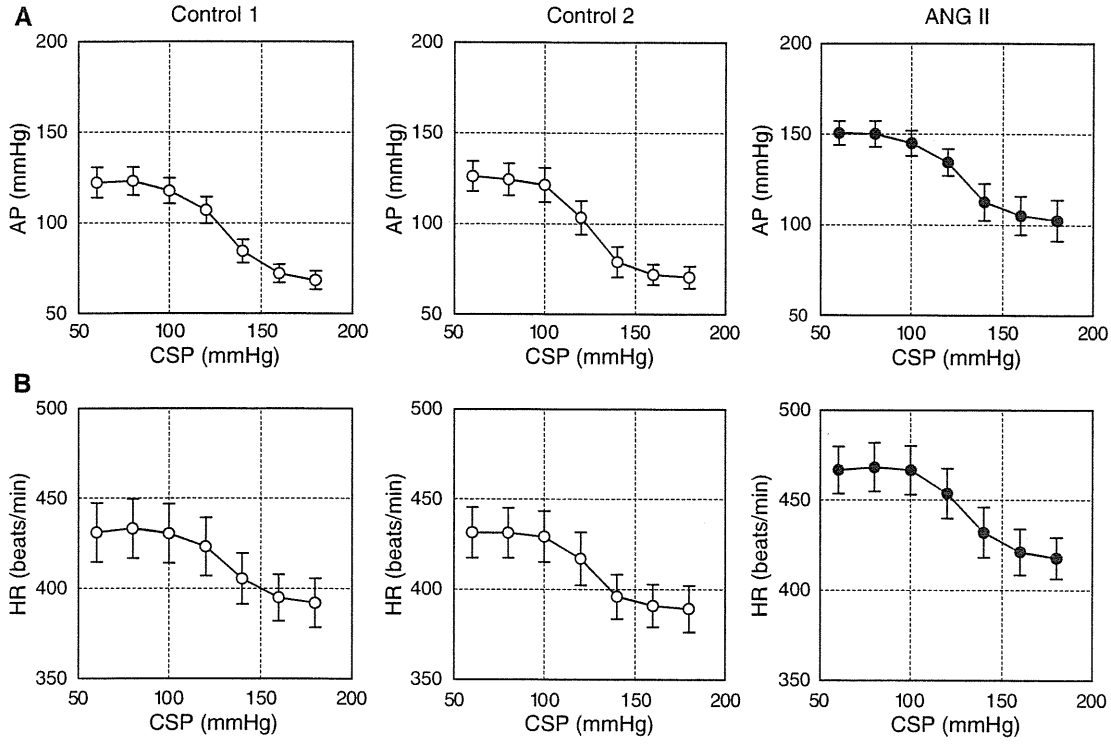

Fig. 2 **a** Averaged input–output relation of the total baroreflex. AP decreased in response to an increase in the CSP. ANG II increased AP, while the range of the AP response was preserved. **b** Averaged input–output relation of the arterial baroreflex control of HR. HR decreased in response to an increase in the CSP. ANG II increased the HR, while the range of the HR response was preserved

unaltered, which agreed with a previous study from our laboratory in which intravenous ANG II at 100 ng kg^{-1} min^{-1} did not change the dynamic gain of the neural arc in anesthetized rabbits [23]. In contrast, Sanderford and Bishop demonstrated that ANG II at 10 or 20 ng kg^{-1} min^{-1} significantly reduced the maximum renal SNA and attenuated the range of baroreflex control of renal SNA in conscious rabbits [9, 24]. On the other hand, Tan et al. [12] demonstrated that intravenous ANG II at 400 ng kg^{-1} min^{-1} did not increase the levels of renal SNA in anesthetized rats. The regional differences in SNA may partly explain the conflicting results, because Fukiyama [25] noted that ANG II infusion (3.5–9.5 ng kg^{-1} min^{-1}) through the vertebral artery resulted in an increase in splanchnic SNA, a transient increase followed by a decrease in renal SNA, and no change in cardiac SNA in anesthetized dogs.

Activation of the renin–angiotensin system contributes to the pathologic sympathoexcitation observed in such cardiovascular diseases as chronic heart failure. In addition to the augmented cardiac sympathetic reflex, impairment of the arterial baroreflex is thought to contribute to sympathoexcitation [13]. The present results indicate that ANG II may increase SNA, but it does not attenuate baroreflex control of SNA such that the magnitude of the SNA response to the input pressure change is preserved (Fig. 3a). ANG II also did not attenuate the gain of the total baroreflex estimated by the magnitude of the AP response to the input pressure change (Fig. 2a). Therefore, the observed weakening of the baroreflex reported in patients with chronic heart failure may not be readily explainable by an acute effect of high circulating levels of ANG II.

Several studies have demonstrated that ANG II-induced hypertension does not decrease SNA via the arterial baroreflex compared to equivalent hypertension induced by phenylephrine [10, 12, 26]. Although those results seem to be consistent with the idea that ANG II blunts the arterial baroreflex, the experimental protocol is confusing, and the interpretation could be wrong as follows. The intersection between the neural and peripheral arcs in the baroreflex equilibrium diagram conforms to the closed-loop operating point [21, 27, 28]. In the present study, ANG II significantly increased AP without significant changes in SNA at the closed-loop operating point (Fig. 4, open vs. filled circles; Table 1). If we calculate the baroreflex control of SNA based on ANG II-induced hypertension, therefore, we would incorrectly conclude that the baroreflex does not control SNA. If we observe the SNA response to changes in